MTL TR 89-78

AD

THE EFFECT OF COMPOSITION AND AGING TREATMENT ON THE MICROSTRUCTURE AND MECHANICAL PROPERTIES OF ALUMINUM-LITHIUM-TITANIUM ALLOYS

MARIETTA R. CAPPUCCI
METALS RESEARCH BRANCH

August 1989

US ARMY
LABORATORY COMMAND
MATERIALS TECHNOLOGY LABORATORY

U.S. ARMY MATERIALS TECHNOLOGY LABORATORY
Watertown, Massachusetts 02172-0001

The findings in this report are not to be construed as an official Department of the Army position, unless so designated by other authorized documents.

Mention of any trade names or manufacturers in this report shall not be construed as advertising nor as an official indorsement or approval of such products or companies by the United States Government.

DISPOSITION INSTRUCTIONS

Destroy this report when it is no longer needed.
Do not return it to the originator.

UNCLASSIFIED

SECURITY CLASSIFICATION OF THIS PAGE (When Data Entered)

REPORT DOCUMENTATION PAGE		READ INSTRUCTIONS BEFORE COMPLETING FORM
1. REPORT NUMBER MTL TR 89-78	2. GOVT ACCESSION NO.	3. RECIPIENT'S CATALOG NUMBER
4. TITLE (and Subtitle) THE EFFECT OF COMPOSITION AND AGING TREATMENT ON THE MICROSTRUCTURE AND MECHANICAL PROPERTIES OF ALUMINUM-LITHIUM-TITANIUM ALLOYS		5. TYPE OF REPORT & PERIOD COVERED Final 6. PERFORMING ORG. REPORT NUMBER
7. AUTHOR(s) Marietta R. Cappucci		8. CONTRACT OR GRANT NUMBER(s)
9. PERFORMING ORGANIZATION NAME AND ADDRESS U.S. Army Materials Technology Laboratory Watertown, Massachusetts 02172-0001 SLCMT-EMM		10. PROGRAM ELEMENT, PROJECT, TASK AREA & WORK UNIT NUMBERS D/A Project 1L162105.AH84
11. CONTROLLING OFFICE NAME AND ADDRESS U.S. Army Laboratory Command 2800 Powder Mill Road Adelphi, Maryland 20783-1145		12. REPORT DATE August 1989 13. NUMBER OF PAGES 99
14. MONITORING AGENCY NAME & ADDRESS(if different from Controlling Office)		15. SECURITY CLASS. (of this report) Unclassified 15a. DECLASSIFICATION/DOWNGRADING SCHEDULE

16. DISTRIBUTION STATEMENT (of this Report)

Approved for public release; distribution unlimited.

17. DISTRIBUTION STATEMENT (of the abstract entered in Block 20, if different from Report)

18. SUPPLEMENTARY NOTES

Thesis submitted to MIT, Department of Materials Science and Engineering, Cambridge, MA, on January 20, 1989 in partial fulfillment of the requirements for the Degree of Master of Science in Metallurgy.

19. KEY WORDS (Continue on reverse side if necessary and identify by block number)

Aluminum-lithium-titanium alloys	Mechanical properties
Lightweight alloys	Transmission electron microscopy (TEM)
Microstructure	Powder metallurgy

20. ABSTRACT (Continue on reverse side if necessary and identify by block number)

(SEE REVERSE SIDE)

DD FORM 1 JAN 73 1473 EDITION OF 1 NOV 65 IS OBSOLETE

UNCLASSIFIED

SECURITY CLASSIFICATION OF THIS PAGE (When Data Entered)

Block No. 20

ABSTRACT

Aluminum-lithium alloys have recently been recognized for their potential as aerospace alloys. Al-Li alloys offer the combination of high strength and elastic modulus with low density, thereby resulting in substantial weight and cost savings. The precipitation of the metastable δ' (Al_3Li) phase upon aging provides considerable increases in strength. The major problem encountered thus far is that the δ' phase, due to its shearable nature, causes slip localization, reducing ductility and fracture toughness. The present study is based on the theory that by altering the precipitation behavior and characteristics by additions of titanium it will be possible to disperse slip and consequently increase fracture toughness. Titanium has been selected as the alloying element because in the Al-Ti binary system Al_3Ti forms with lattice parameter and crystal structure similar to those of Al_3Li.

Al-3Li, Al-3Li-0.2Ti and Al-3Li-0.8Ti (wt%) alloys were processed using powder metallurgy and were extruded. Microstructural characterization at various age hardening conditions has been carried out. A ternary $Al_3(Li,Ti)$ phase, designated α', precipitates upon solution heat treatment at 500 C for 24 hours. α' precipitates as a coherent ordered precipitate with high matrix coherency strain. Upon aging, δ' precipitates both homogeneously in the matrix and heterogeneously at the α'/matrix interface, forming a "composite" precipitate consisting of an α' core surrounded by δ'. The technique of superlattice dark field image calculation has been used to determine the composition of the $Al_3(Li_x,Ti_{1-x})$ phase. The value for x has been determined to be ~ 0.4 - 0.6.

The mechanical properties of the alloys have been determined at several aging conditions. The strength of the alloy increases significantly at each aging condition as titanium is added to the system. Elongation to failure remains fairly constant with titanium additions, but fracture toughness drops as higher amounts of titanium are added. The Al-3Li-0.2Ti alloy shows the best combination of strength and toughness.

TABLE OF CONTENTS

Page

LIST OF FIGURES

LIST OF TABLES

ACKNOWLEDGEMENTS

The funding for this thesis was provided in its entirety by the Army Materials Technology Laboratory in Watertown, MA. I would like to thank Dr. Paul Fopiano, Dr. Eric Kula, Dr. Martin Wells and Dr. Ralph Adler for their support.

I would like to thank Professor John B. VanderSande for serving as MIT advisor to this thesis.

There are many people at MTL without whom this thesis could not have been completed. I'd like to thank Andy Zani, the staff of the Print Shop, the Mechanical Testing Laboratory and the Machine Shop, in particular, Lenny Bucciarelli, Jack Kelley and Jim Wong.

I'd like to thank Ernest S.C. Chin for his assistance with the procurement of the materials and for his helpful discussions. Thanks also go to Becky Weiss and Jonathan Montgomery for their advice, and to Robert Huie and Steve Oliver for their support and friendship.

Extra special thanks go to my Mom and Dad, Auntie Kay, and Katy, Anna, Marian and Joey for always encouraging me and being there for me.

Most importantly, huge amounts of love and appreciation go to James Frederick Scanlon for his constant love, support and tolerance over the course of this work, and for all his help in putting together the final product.

INTRODUCTION

Lithium-containing aluminum alloys, although first investigated in the early 1920's, have just recently been recognized for their potential as aerospace alloys. Aluminum-lithium alloys offer a desirable combination of higher strength and elastic modulus in conjunction with reduced density as compared to conventional aluminum alloys.[1,2] It has been shown that each additional weight percent lithium added to aluminum will decrease the density by 3 percent while increasing the elastic modulus by 6-8 percent .[3-5]

Lithium additions, as well as increasing the elastic modulus, also provide considerable increases in strength due to the precipitation of a metastable δ' phase. The δ' phase precipitates as an ordered Cu_3Au ($L1_2$) type simple cubic crystal structure. A small lattice misfit exists between the α and δ' phases resulting in a small misfit strain, which therefore results in precipitation of δ' as spherical, coherent particles.

Low density, high modulus, high strength properties afforded by lithium additions make Al-Li alloys desirable for use in structural applications in the aerospace industry as well as armor applications for military vehicles, while providing substantial weight and cost savings over conventional aluminum alloys.

The major obstacle in the commercialization of aluminum-lithium alloys is the low ductility and fracture toughness exhibited by the alloys. These detrimental properties have been attributed mainly to the precipitation of the δ' phase. The primary mechanism for increase in strength is order hardening, by which the ordered δ' precipitates are sheared by dislocations.[11] The shearing results in slip localization and stress concentrations at grain boundaries, consequently reducing fracture toughness.[4-10] Several investigators have attempted to alter the mechanism of dislocation shear with alloying additions designed to coprecipitate with δ'.[6,7,12-16] The major alloying additions examined thus far have been titanium, zirconium and hafnium.

In the present study, attempts are made to improve toughness and ductility of the alloys with titanium additions. The major influences behind this work were recent studies performed by Gayle[12] who investigated zirconium additions, and Levoy,[16] who investigated both titanium and hafnium additions. Results of these studies indicated that improvements can be realized due to the additional alloying elements.

Titanium was chosen as an alloying element for this work because titanium forms the Al_3Ti phase with the DO_{22} crystal structure, and a lattice parameter similar to that of the

Al_3Li phase. Ti additions result in the precipitation of a modified δ' $Al_3(Li,Ti)$ phase, designated α', with the $L1_2$ ordered structure.[16] If the precipitation of this α' phase results in improved behavior during deformation, then the fracture toughness of the alloys can be increased while retaining the benefits of the lithium additions.

The primary goals of this research are to :

1. Determine the effects that composition and thermal treatments have on the microstructure and precipitation behavior of the alloys.

2. To compare mechanical properties and behavior of the system in response to the compositional and thermal variations.

Al-3Li, Al-3Li-0.2Ti and Al-3Li-0.8Ti (wt%) powder metallurgy alloys were investigated. Microstructural analysis was performed through transmission electron microscopy. Mechanical tests were performed to provide tensile and fracture toughness data.

SURVEY OF CURRENT LITERATURE

History

The development of lithium-containing aluminum alloys has been continuing for more than sixty years. The first aluminum-lithium alloys were developed as early as 1920, with the introduction of Scleron, an Al-Zn-Cu-Li alloy developed in Germany for use as a casting alloy and in wrought forms. The alloy did not exhibit superior properties over conventional alloys of the time and did not see much use. It was not until 1942, when Lebaron of Alcoa applied for a patent on Al-Cu-Li-X alloys, that the system's potential for high strength was realized. However, at that time alloy 7075 had been introduced and was established as the dominant system for strength applications, and interest in the Al-Cu-Li system again receded. In 1958, spurred by the publication of several papers on Al-Li alloys,[17-19] Alcoa developed the Al-Cu-Li-Mn-Cd alloy X-2020.[20] This alloy exhibited high tensile properties and elastic modulus, and the aerospace industry recognized the potential of 2020. The U.S. Navy's A-5A and RA-5C Vigilante, built by Rockwell International, was the only production application for alloy 2020. The upper and lower skins on the wings and the horizontal stabilizer were originally designed with 7075-T651 plate. These parts were changed to 2020-T651 in 1958 and have experienced a successful service history. Alloy 2020 was evaluated for other applications, none of which were used due to concern over fracture behavior of the alloy.[20] Because of the general reluctance of industry to get involved with Al-Li alloys, virtually all further development of the alloys ceased after 1964.

It was not until 1968 that Fridlyander patented 01420, with composition Al-5Mg-2Li-0.5Mn.[21] It was only after the introduction of this alloy that a complete investigation of the δ' (Al_3Li) phase, its precipitation characteristics, and deformation behavior was initiated.[22] Peel, et. al.. began an alloy development program in 1977[14] aimed at producing a series of new Al-Li alloys which met specific requirements of use in aerospace structures. Results of their research indicated that the reduction in density and increase in stiffness achieved by Al-Li alloys were sufficient to produce substantial weight savings against conventional Al alloys. Pickens, et. al.,[23] have also recently investigated high strength aluminum alloy development. High strength, high modulus, low density ingot metallurgy (I/M) and powder metallurgy (P/M) Al-Li alloys were investigated as potential

replacements for conventional Al alloys such as 2014, 2024, and 7075. Al-Li alloys close to commercialization are 2090,[24] 2091,[26] 8090 and 8091.[25]

Starke, et. al., [27] have also investigated the development of P/M and I/M Al-Li alloys with the discovery of significantly improved modulus-to-density and strength-to-density ratios as compared to 7075-T76 without significant loss in other properties.

The development and evaluation of Al-Li-Cu-Mg, Al-Li-Mg and Al-Li-Cu alloys has been carried out by Bohlen and Chanani of Northrop Corporation.[15] Powder and ingot metallurgy techniques were used for production. Results of this work indicate that it is possible to create Al-Li systems with 10% lower density and strengths equivalent to or exceeding 7075-T73, again indicating potential use by the aircraft industry.

As the δ' phase is further investigated, a better understanding of the mechanical and metallurgical properties of these Al-Li alloys is achieved. This progressive understanding of Al-Li alloy properties has led to constant improvement of the alloys, and most recently producers are increasing production in anticipation of continued growth and use by aerospace markets. These property improvements will make aluminum-lithium alloys suitable for a wide variety of applications. Companies such as Boeing, Textron Inc's. Aerostructures unit, Inco, and Pechiney are all developing Al-Li alloys for a variety of aircraft applications at substantial weight and cost savings.[28]

The Al-Li Binary System

The addition of lithium to aluminum produces an age-hardenable alloy. The precipitation sequence is known to be,[29]

$$\text{Supersaturated solid solution} \text{ -------> } \delta' (Al_3Li) \text{ ------> } \delta (AlLi)$$

This sequence occurs in alloys containing <14 at% Li. The Al-Li binary phase diagram is illustrated in Figure 1.[30] In Figure 1 it is clear that the maximum solubility of Li in FCC aluminum at the 600 C eutectic temperature is 13.8 at%. The eutectic reaction at 600 C is:

$$\text{Liquid} \text{ -------> } \alpha (Al) + \delta (AlLi)$$

with Li compositions, in atomic percent, being 26, 14, and 45, respectively.

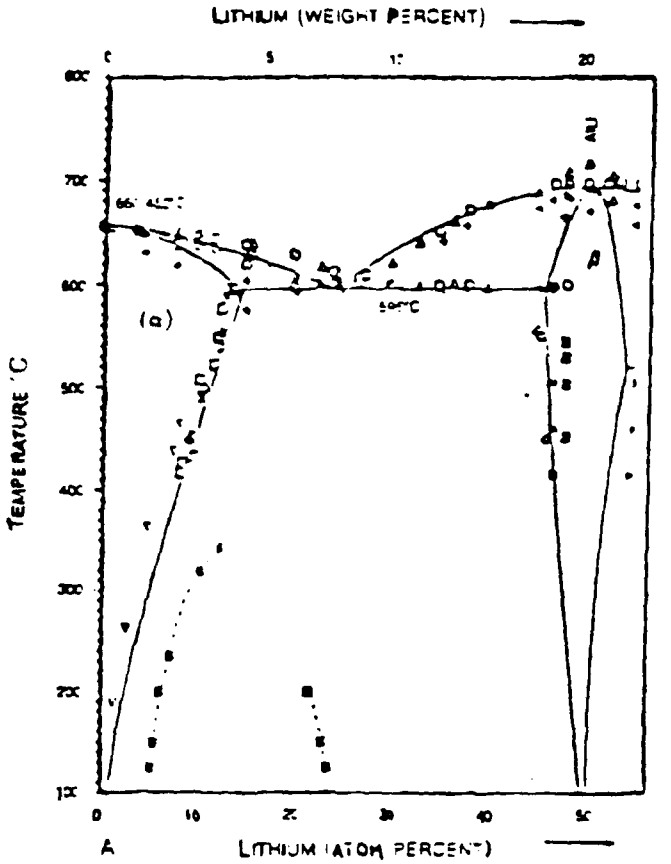

Figure 1 *Binary Al-Li Phase Diagram Including Metastable α + α' Phase Field.*

The δ phase forms as a cubic B_{32} NaTl-type structure. The δ phase melts congruently at 700 C with a solubility range of 45-55 at% Li. The lattice parameter of δ is 6.37 Å.[30]

The phase diagram of Figure 1 includes metastable coherent solvus lines for α-Al and α'. α' is the ordered $L1_2$ Al_3Li phase more commonly designated δ' by aluminum metallurgists. This α-α' system has not yet been thoroughly defined. However, reliable values for the thermodynamic δ' solvus have been attained by small-angle X-ray scattering and the entire coherent miscibility gap has been computed by Cocco, et. al.[31] This work complimented previous work performed by Noble and Thompson in 1971.[29] The phase diagram for the α-α' system as obtained by Cocco, et. al., is illustrated in Figure 2. This diagram has been generally accepted, however, an alternate phase diagram has been proposed by Gayle and VanderSande,[12] and is shown in Figure 3. The rationale behind the alternative diagram is based on the fact that the Al-->$L1_2$ transformation is first order and thus, a two-phase field separating the α and α' phase fields must exist. Gayle's construction has been accepted as plausible[32] and still allows for either spinodal decomposition or homogeneous nucleation to occur.

The δ' Phase

As was shown in the phase diagram, a metastable miscibility gap exists between the α-Al phase and the δ' (Al_3Li) phase. The δ' phase precipitates as an ordered Cu_3Au ($L1_2$) type simple cubic crystal structure. The $L1_2$ structure is derived from an ordering of the face centered cubic cell (See Figure 4).[33] The α and δ' phases have a similar structure and a small lattice misfit of δ', which has been determined to be approximately -0.08%.[34,35] The precipitate-matrix interfacial energy was determined to be approximately 0.014 J/m^2.[36] The small lattice misfit results in a small misfit strain and therefore the δ' phase precipitates as a spherical coherent precipitate and remains as such over a wide range of dimensions and lithium supersaturations.[37]

It has been disputed whether the δ' phase forms upon quenching. Noble and Thompson, and Fridlyander et. al.[29,38] report no δ' in the as-quenched condition, while other investigators have observed δ'.[35,39-41] Also, a question which remains unresolved is whether or not δ' forms by homogeneous nucleation and growth, or spinodal decomposition.[43]

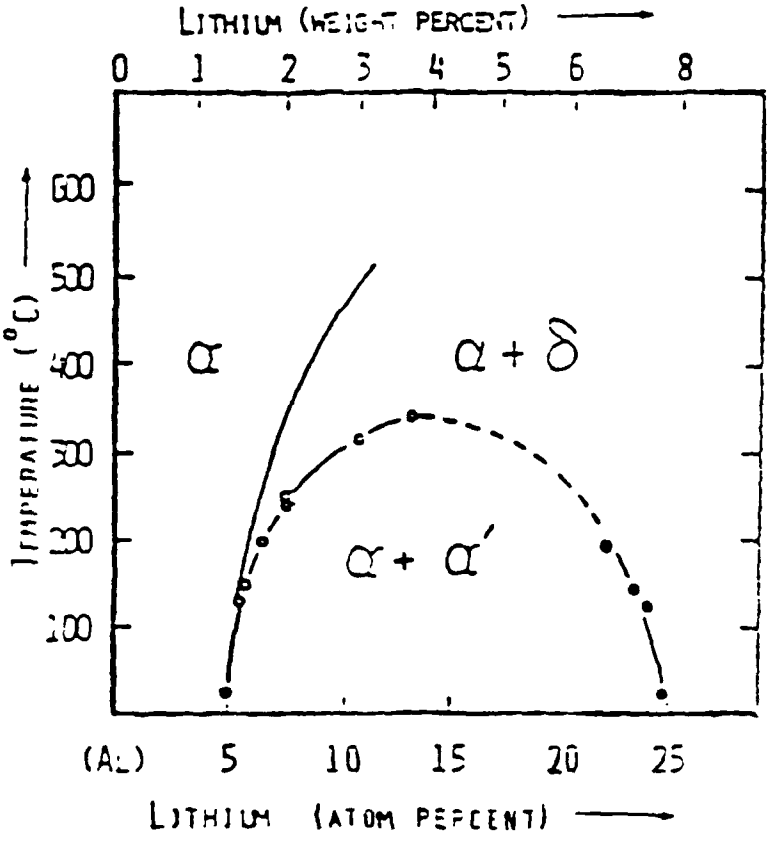

Figure 2 $\alpha + \alpha'$ *System as Generally Accepted In Recent Literature*

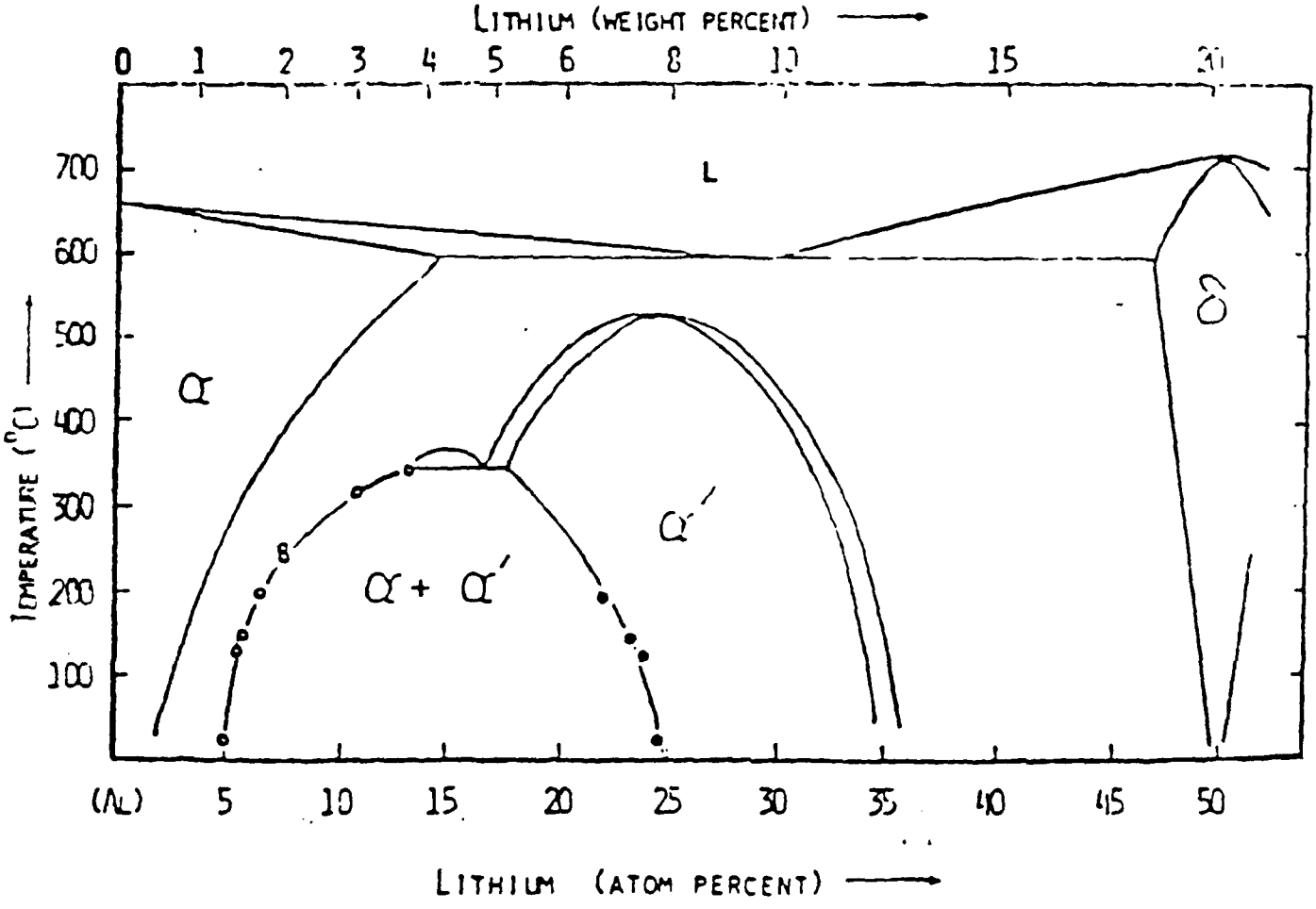

Figure 3 Newly Proposed α + α ' System.

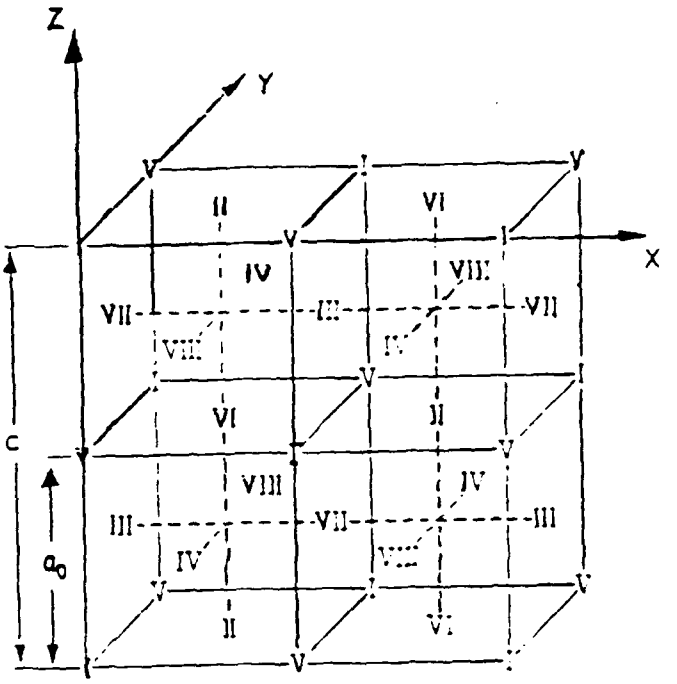

Designation	Spacegroup	Basis	Positions	Occupation
$L1_2$	Pm3m (cubic)	$a=a_o\{100\}$	1 a(000) 3 c(0,1/2,1/2)	I=V II=III=IV=VI=VII=VIII

Figure 4 *$L1_2$ structure derived from an ordering of the face centered cubic cell.*

Strengthening Behavior

As the δ' phase forms, a significant increase in the alloy's strength is achieved.[6,12,16,44] The δ' phase gives the Al-Li alloys their precipitation hardening capability and assigns the alloys their principal microstructural characteristics.

Artificial aging at 190 C or some temperature within the α-δ' system causes the δ' to coarsen homogeneously in the matrix according to standard Ostwald ripening kinetics,[12,16,42,43,45,47] with the relationship $r = kt^{1/3}$. The δ' phase also coarsens heterogeneously at the grain boundaries or on dislocations.[43] During homogeneous coarsening the δ' generally maintains its spherical shape, however Mahalingam, et. al.[45] report that as the amount of lithium increases, the δ' particles diverge from the spherical morphology, which is brought about by coalescence among adjacent particles. A discontinuous precipitation reaction has also been observed at the grain boundaries.[43,48] In this case, the spherical precipitates are converted to lamellae. The δ' lamellae maintain coherency with the matrix. The driving force for the reaction is the reduction of the α/δ' surface energy. Whether or not the lamellae form depends greatly on several factors, including the number of alternate heterogeneous nucleation sites and the state of anneal of the material.[43]

The δ-δ' Interaction

The cubic B_{32} NaTl-type structure δ (AlLi) phase has been observed in the matrix and on grain boundaries after continued aging.[49,50] It has been found that the δ precipitate nucleates and grows and is surrounded by a dislocation network caused by the large lattice mismatch between δ and the matrix. The δ precipitates are also surrounded by a δ' precipitate free zone (PFZ). The more stable nature of δ accounts for the preferential dissolution of the nearby δ'. The δ' PFZ grows by a solute depletion mechanism and the δ' solute is consumed during the growth of δ at the grain boundary. The PFZ growth is a diffusion controlled process, with the activation energy of the PFZ growth calculated to be 144 kJ/mol.[51] The growth of the PFZ has been fitted to a parabolic growth law. The formation of the δ' PFZ along the grain boundaries results in an intergranular weakness which can limit ductility and reduce age hardening properties after extended periods of time.

Mechanical Properties And Deformation Behavior

As discussed above, Al-Li alloys have greater potential for aerospace applications due to the alloys' high strength, high modulus and low density. What is obstructing rapid integration of these alloys into current systems is the low ductility and low fracture toughness values that the alloys exhibit. Before Al-Li alloys can be successfully utilized, the causes of low ductility and fracture toughness must be recognized and rectified. There has been much research and investigation into the problems and it is generally agreed upon that the precipitation of the metastable δ' phase has a direct influence on the less than adequate mechanical properties.

As mentioned previously, the addition of each weight percent of Li to Al will decrease the density by three percent, resulting in an 8-10% reduction in weight, while increasing the elastic modulus by approximately 6-8%.[3-5, 42] The strength of Al-Li alloys with less than 4 wt% lithium increases as the percent of lithium is increased, whereas at greater than 4 wt% Li, the brittle δ phase forms and lowers the tensile strength.[3] The strength of the alloys also increase in response to aging time until a peak age is reached, however, a concurrent loss in ductility also occurs.[13,42,52-56]

Noble, et. al.[3] determined the major strengthening mechanism to be order hardening with additional minor contribution by modulus hardening. This was later confirmed by DeHossen and Veld.[57] In Al-Li alloys dislocations are present as superdislocation pairs, which move along {111} planes in close-packed directions.[58] The dislocations pass through the matrix, with their movement depending upon the size and volume fraction of the δ' precipitates.[59] For particles less than approximately 20 nm, a dislocation in the pair shears the particle creating a high energy anti-phase boundary (APB) which blocks dislocation movement and increases strength. The second dislocation then moves through, recreates order, and reduces the APB size and energy.[5,9,10] This dislocation motion encourages planar slip, i.e. strain localization. The extent of the strain localization depends on the change in flow stress between one region and another, implying that increasing the lithium content or aging to peak age will increase the yield stress and therefore increase the degree of slip concentration.[6] The strain localization will lead to cracking on the slip bands, or produce a dislocation pileup along the grain boundary, which can result in intergranular fracture.[6] A schematic of the shearing process is illustrated in Figure 5. Upon aging, the δ' precipitates coarsen, as detailed in the previous section. As the δ' increase in size to greater than approximately 20 nm, the dislocations passing through bow out and become wavy. The dislocations eventually form Orowon loops[60]

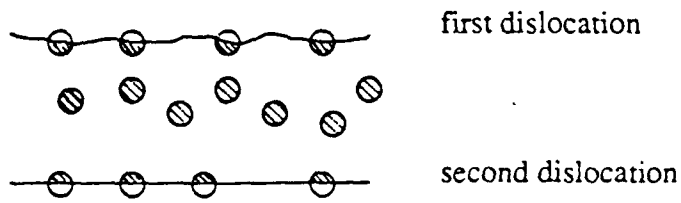

Figure 5 *Schematic representation of dislocations shearing particles and creating a high energy anti-phase boundary (shaded region).*

around the δ', which results in overaging and softening of the alloy. A schematic of the looping process is indicated in Figure 6.

The Aluminum-Titanium Binary System

The principal use of titanium in aluminum alloys is to refine the grain size by precipitation of the Al_3Ti intermetallic. Much of the literature has been devoted to investigating titanium's role as a grain refiner.[61-67] More limited information is available on the mechanical properties and deformation behavior of the Al-Ti system and Al_3Ti.

The Al-Ti binary equilibrium phase diagram is illustrated in Figure 7.[89] Of particular interest are the temperature dependence of the solubility of titanium and the Al_3Ti peritectic reactions. The equilibrium solid solubility of Ti varies from 1.15 wt% at 665 C to approximately 0.2 wt% at 500 C, indicating that it is greatly dependent on temperature. At 665 C a peritectic reaction occurs in which the liquid contains 0.15 % Ti and the solid solution contains 1.2 % Ti:

$$\text{Liquid} + Al_3Ti \text{ -----> } \alpha_{ss}$$

The Al_3Ti compound forms by peritectic reaction at 1340 C. Equilibrium Al_3Ti has a DO_{22} cubic tetragonal structure,[68-70] as illustrated in Figure 8. The cell is composed of two distorted $L1_2$ subcells stacked on top of one another along the [001] direction, with a shift of 1/2<110> on the (001) plane at their interface.[69]

In an as-cast alloy, the Al3Ti phase precipitates in the form of dendrites surrounded by a thin layer of α-Al.[61] They have also been described as laths and irregular plates,[68] petal-like,[64,67] blocky, and flake-like.[67]

The Al_3Ti phase is slow to form.[68] Possible explanations for this are the large lattice misfit of Al_3Ti with the α-matrix and the absence of a coherent intermediate phase.[68] Another explanation is the low rate of diffusion of titanium in aluminum. Elemental diffusion data and intermetallic properties of the Al-Li and Al-Ti systems are listed in Table I.

Deformation Behavior In Al-Ti Alloys

Limited information is available on the mechanical properties and deformation behavior of the Al-Ti system. A decrease in the yield stress as a function of temperature

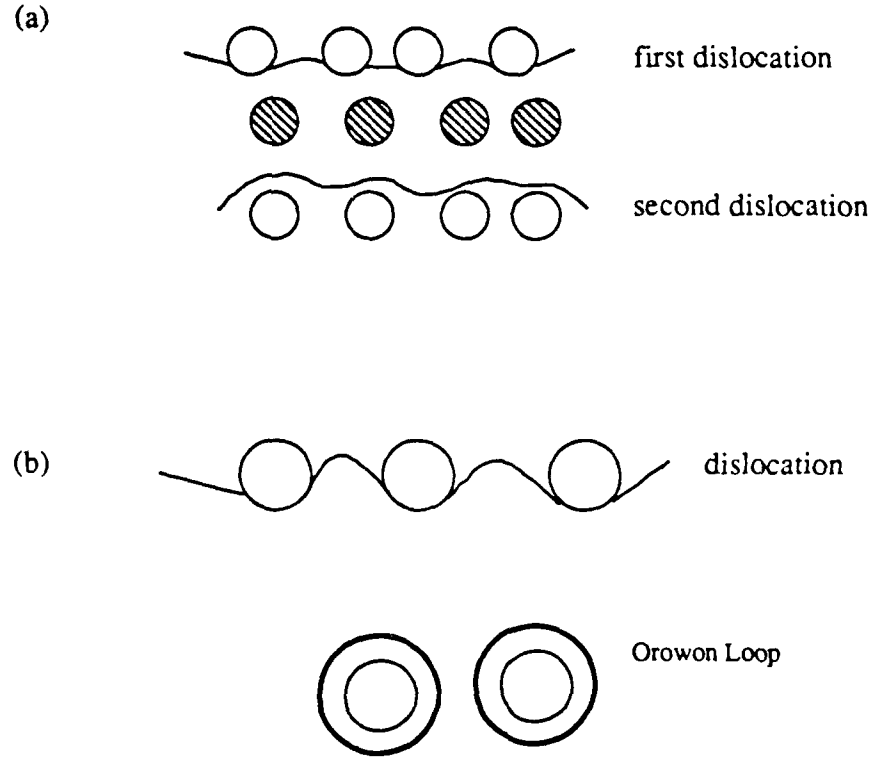

Figure 6 *Schematic representation of precipitate - dislocation interactions. (a) Dislocations bowing around peak-aged precipitates. (b) Orowon loops forming around over-aged precipitates. (Shaded region is anti-phase boundary.)*

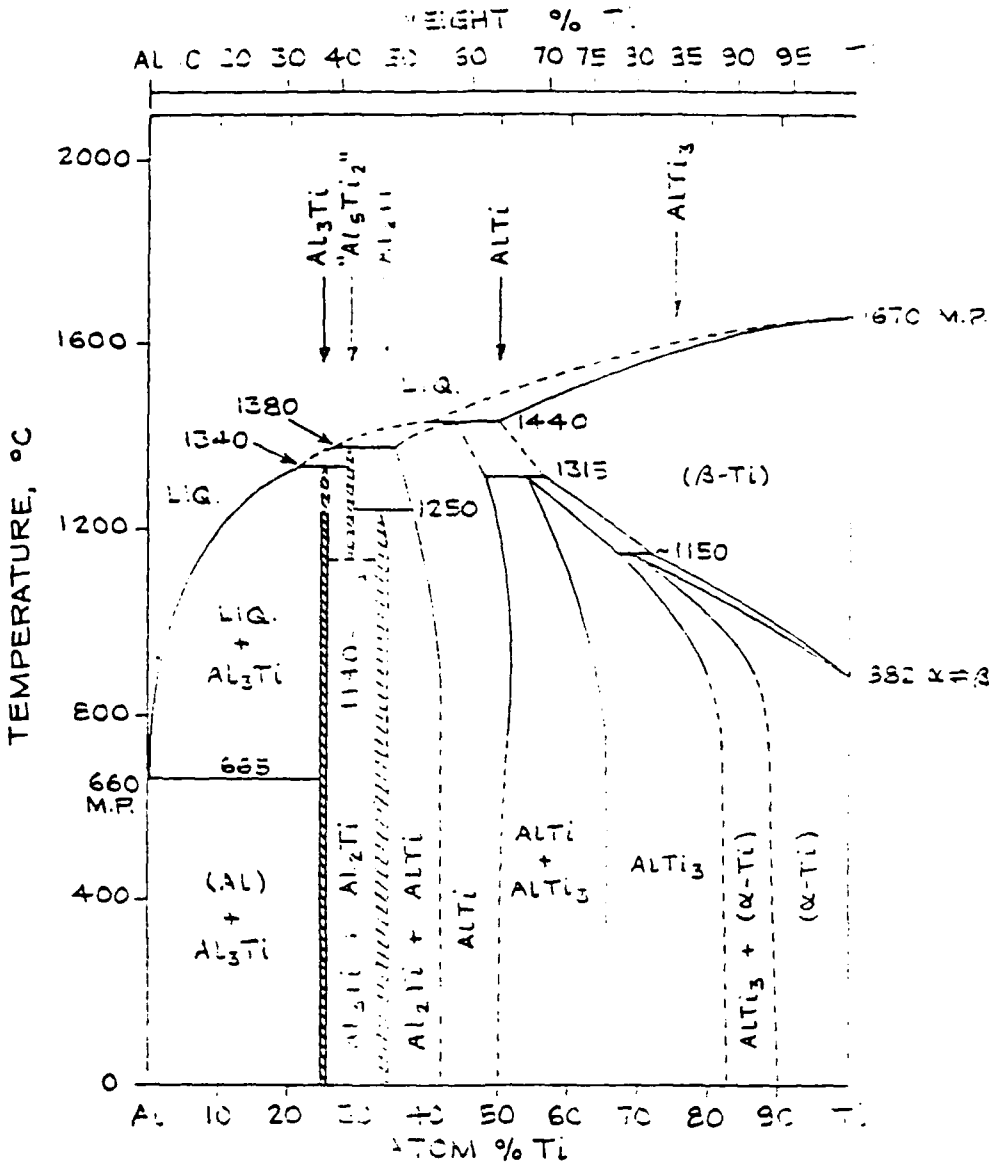

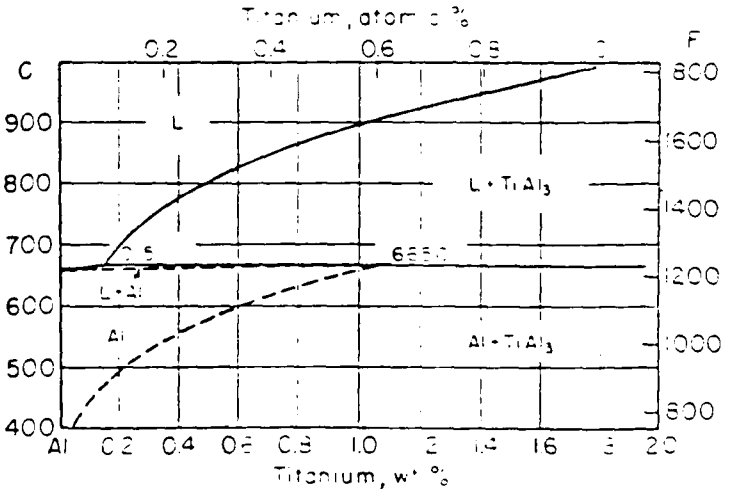

Figure 7 (a) Aluminum-Titanium binary phase diagram. (b) Enlarged view of aluminum-rich end of diagram.

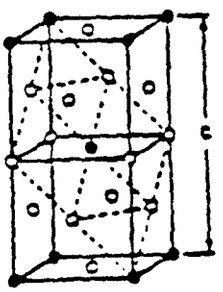

FIGURE 8 DO_{22} Cubic Tetragonal Structure.

TABLE I **RELEVANT PROPERTIES OF ELEMENTS AND INTERMETALLIC PHASES IN Al-Li AND Al-Ti SYSTEMS**
(references in parentheses)

PHASE [structure]	LATTICE PARAMETER (Å)	LATTICE MISFIT (Δ%)	INTERFACIAL ENERGY (erg/cm²)	MODULUS (Δ%/wt%)
Al_3Li $[L1_2]$	4.047(35)	-0.08(35)	25 (35)	7-9 (4,5)
Al_3Ti $[DO_{22}]$	a=3.851(90) c=8.608	-1.35 (12)	——	3.7 (90)

ELEMENT	D_0(cm²/sec)	Q(kJ/mole)	D_x (190 C)	D_x (500 C)
Li	4.5	138	1.2×10^{-15}	2.1×10^{-9} (91)
Ti	5×10^{-7}	108	3.2×10^{-19}	2.5×10^{-14} (90)

has been observed by both Williams and Blackburn and Lipsett et. al.[71,72] The drop has been attributed to the onset of dislocation climb. However, Sastry et. al. have reported an increase in the fracture tensile stress with temperature.[7] Frazier and Koczak[74] determined that fine Al_3Ti particles precipitate during thermal exposure, increasing hardness.

The Al-Li-Ti Ternary System

The ternary Al-Li-Ti system has yet to be studied extensively and limited information is available on microstructural and mechanical properties. Because Al-Li alloys have less than satisfactory ductility and fracture toughness due to the formation of strain localization, it has been suggested that these alloys be modified by the addition of a transition element such as Ti, Zr or Hf.[75] The additions of such a transition element result in an altered precipitation hardening behavior and consequent increase in toughness.

Levoy[16] confirmed that the addition of Ti to Al-Li alloys results in the precipitation of a ternary $Al_3(Li,Ti)$ phase with the $L1_2$ ordered structure. The phase is denoted α'. α' forms as coherent, spherical particles with large matrix coherency strain. Upon further aging, α' acts as a heterogeneous nucleation site and δ' precipitates preferentially at the α'/matrix interface.

Sankaran et. al.[76] have observed a homogeneous deformation substructure in Al-Li-Ti alloys in contrast to the intense planar slip observed in binary Al-Li. Sankaran et. al. conclude that the dispersoid particles formed in the ternary alloy interact with the dislocations which result in dislocation debris at the particles causing slip dispersion and increased ductility.

Fracture Behavior

As mentioned, the deformation behavior of Al-Li is by formation of planar slip bands and grain boundary failure. The fracture behavior has been found to vary with the alloys' aging condition. Fracture in binary alloys tends to be intergranular due to dislocation pileups at grain boundaries, and grain boundary denuded zones.[27,77]

OUTLINE AND PLAN OF WORK

The objectives of the present research are twofold. The first objective is to determine the effects compositional variations and thermo-mechanical treatments have on the microstructure and precipitation behavior in alloys of the Al-Li-Ti system. The second objective is to determine changes in mechanical behavior of the system in response to these compositional and thermal variations. A general outline of the approach is illustrated in Figure 9.

Alloys with the nominal compositions Al-3%Li, Al-3%Li-0.2%Ti and Al-3%Li-0.8%Ti (wt%) were chosen for the study. A rapid solidification process of inert gas atomization was performed to produce the alloys with the desired Li and Ti supersaturations. Following the atomization, the alloys were consolidated by hot compaction and extrusion. These processes were performed at temperatures low enough to maintain the supersaturated solid solution.

Thermal treatments were performed and the general relationship between heat treatment, precipitation behavior, and mechanical properties was investigated using hardness versus aging curves, transmission electron microscopy (TEM), and tensile and fracture toughness testing.

Microstructures of the alloys were characterized using the TEM techniques of bright field and superlattice dark field imaging and selected area diffraction. Elongation to failure, tensile and yield strengths, as well as fracture toughness were reported as a function of thermal treatment.

Fracture surfaces of the test specimens were analyzed using scanning electron microscopy (SEM) to determine the effects of composition and heat treatment on fracture behavior.

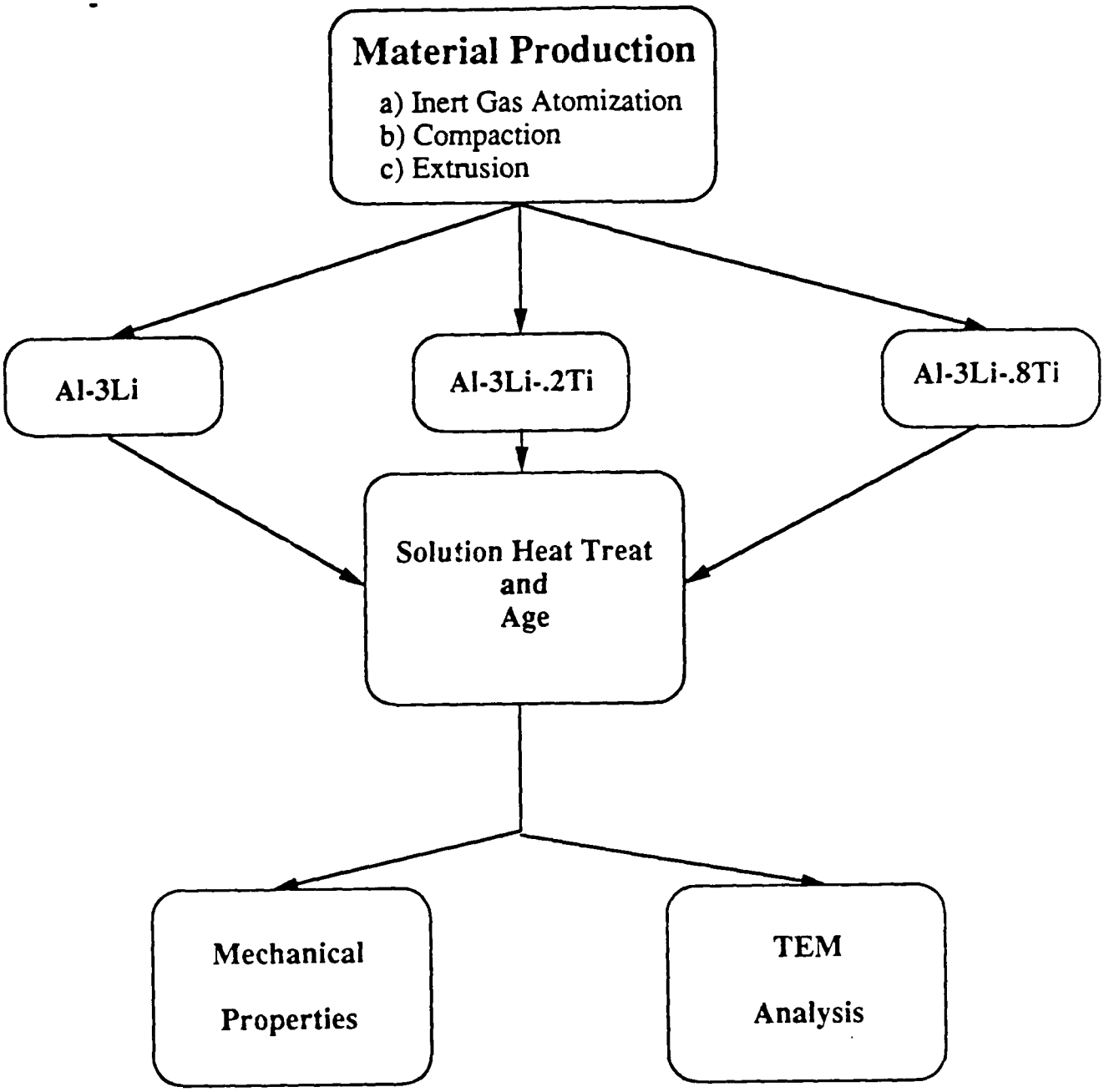

Figure 9 Outline of Approach

EXPERIMENTAL PROCEDURE

Material Production

Inert Gas Atomization

Inert gas atomization at a temperature above the liquidus of the high titanium alloy was used to prepare the alloys. The alloys were inert gas atomized by Homogenous Metals, Inc. (Herkimer, NY). Blow temperatures for the alloys were 1635 F for the binary alloy, 1730 F for the low titanium alloy and 1660 F for the high titanium alloy. Each of the alloys was produced from pure elements. Final compositions of the powders were determined to be Al-2.83Li, Al-2.98Li-0.17Ti and Al-2.55Li-0.7Ti (wt%). The powder was sieved and the -100 mesh powder was used for further processing.

Compaction

The powder of each alloy was compacted and extruded by Nuclear Metals, Inc. (Concord, MA). The -100 mesh powders were compacted in a 6061-T6 can. Can weight was 4.10 lbs. with a compact height of 10". Compact and can weight was 17.37 lbs. for the binary and low titanium alloys and 16.75 lbs. for the high titanium alloy. Evacuation was performed at 350 C for a maximum of 4 hours with a cold vacuum of 0.1 μm and a seal vacuum of 0.01 μm. Compaction was performed under a force of 260 tons and a unit pressure of 26.5 ksi.

Extrusion

In order to keep all of the titanium in solution for each of the alloys, the processing temperature was maintained at 304 C, with the liner temperature and die temperature both at 350 C. The rods were extruded to a final shape of 1" x 1.5" x 6' at a 30:1 ratio and a ram speed of 15 rpm.

Thermal Treatments

The extruded bars were examined at various heat treatments as determined by studying aging behavior. Aging curves were determined by aging at 190 C in air and monitoring responses with Rockwell B hardness measurements.

Solution heat treatment was carried out at 500 C for 24 hours. The extruded bars were heat treated in an argon atmosphere and subsequently water quenched. Following solution treatment, the alloys were aged at 190 C in air for periods of time varying from 1 to 24 hours.

Analysis

Transmission Electron Microscopy

Following thermal treatment, samples for TEM were prepared as 3 mm discs. Initial rough grinding was done using 600 grit SiC paper. Final polishing was performed using a twin-jet electropolisher with a solution of 30% nitric acid in methanol. Parameters for polishing of T=-18 C, V=11 volts, I=30 mA, produced acceptable samples for TEM observation. Microscopy was performed on a Phillips 400T TEM. Measurement of percent area of phases was performed on a Buehler Omnimet II Image Analysis System.

Mechanical Testing

Tensile specimens were ASTM standard TR6[78] 0.113" gage diameter round threaded specimens. ASTM standard TR18[79] 0.252" gage diameter crush ground button head specimens were also tested. TR6 tension specimens were tested on a 20K Instron, with a 1/2-10% extensometer. Testing was performed at room temperature with crosshead speeds varying from 0.005-0.01 in/min and load range varying from 500-1000 lbs. depending on the specimen. TR18 tension specimens were tested on a 50K Instron with a load range of 5000 lbs. The crosshead speed was 0.02 in/min.

Fracture toughness values were obtained using fracture toughness bend specimens. Longitudinal test specimens were of width 0.5". Transverse test specimens had a width

equal to 0.45". The notch was a simple notch with a fatigue crack of 0.05". Precracking was done on a MTS servohydraulic machine. Three point point bend testing was performed in the Physical Metallurgy testing machine at a head speed of 0.0125 inch/min.

Scanning Electron Microscopy

Fracture surfaces of the fracture toughness specimens were examined after testing. Fractography was performed on an Amray 1645 SEM with an EDAX Energy Dispersive X-Ray Spectrometer attachment.

RESULTS

Aging Behavior Of Alloys

Age-hardening and precipitation behavior of Al-Li alloys have by studied by several investigators.[11,29,35,48,49,53,80-82] The general aging process is determined to be due to the precipitation of the δ' phase as a coherent quasi-equilibrium phase of $L1_2$ structure.[59] The alloys were solution treated at 500 C for 24 hours followed by subsequent aging at 190 C for various times. Rockwell B hardness values of the Al-3Li, Al-3Li-0.2Ti, and Al-3Li-0.8Ti alloys are plotted as a function of aging time in Figure 10.

The curves in Figure 10 indicate that the Al-Li binary alloy exhibits the fastest response to aging when compared to the ternary alloys. The low Ti alloy responds more slowly than the binary alloy, but more rapidly than the high Ti alloy. The high Ti alloy did not respond as quickly, however, it did have greater hardness in the as-quenched condition and achieved greater hardness values than the other two alloys at equivalent aging conditions.

It is clear from the curves in Figure 10 that a maximum hardness is obtained in the binary alloy after 5 hours at 190 C. Maximum hardness for both the high and low Ti alloys was achieved after aging for six hours. In each case the alloy softens upon further aging.

It is from the study of aging behavior that parameters in Table II for under-aged, peak-aged and over-aged conditions were decided upon for further characterization.

Microstructural Characterization:

Al-Li

The binary Al-Li alloy was examined in the experimentally determined solutionized, under-aged, peak-aged and over-aged conditions (see Table II).

After a solution treatment of 500 C for 24 hours, the alloy exhibits a homogeneous microstructure. Grains observed are relatively equiaxed, with grain size ranging from 4 μm to 15 μm, the average grain size being 9 μm. The lithium remains in solution after

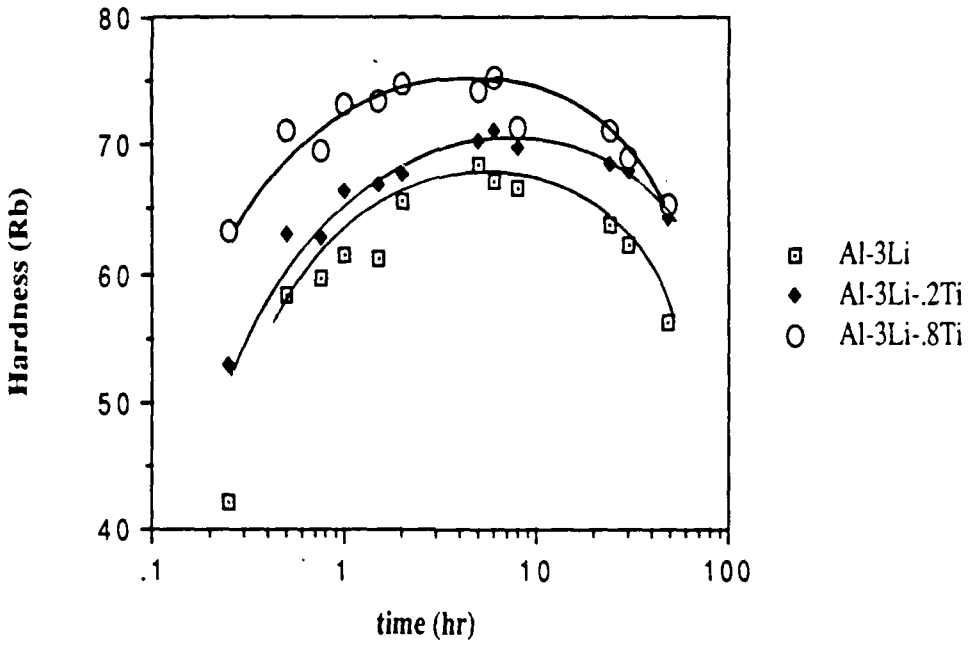

Figure 10 Aging curves for the three alloys. Aged at 190 C.

TABLE II TIME TO ACHIEVE EACH AGING CONDITION

AGING CONDITION	ALLOY	TIME
Under-aged	1,3,6	1 HR.
Peak-aged	1	5 HRS.
	3	6 HRS.
	6	6 HRS.
Over-aged	1,3,6	24 HRS.

(1=Al-3Li, 3=Al-3Li-0.2Ti, 6=Al-3Li-0.8Ti)

heat treatment. A solid solution exists and no precipitation of the δ' phase occurs (Figure 11).

Upon heat treating at 190 C for one hour, the δ' Al_3Li phase begins to precipitate as the $L1_2$ ordered superlattice phase. Formation of δ' occurs by classical nucleation and growth kinetics, although spinodal decomposition may also occur.[1] The δ' phase is nucleated as spherical coherent precipitates. The average size of the δ' phase after aging for one hour at 190 C is 10 nm (Figure 12). Grains in the under-aged binary alloy remain relatively equiaxed, and have an average diameter of 7 μm.

After aging the alloy for six hours at 190 C, peak age has been reached. As illustrated in Figure 13 the δ' precipitates coarsen upon aging. The δ' images brightly in the superlattice dark field condition. The δ' phase has coarsened to an average diameter of 16.5 nm. The average grain size for the peak-aged binary alloy is 7 μm.

Aging the binary alloy at 190 C for 24 hours results in an over-aged condition as indicated by the drop in hardness in Figure 10. The majority of the δ' phase remains spherical and has coarsened to the average size of 33 nm (Figure 14). Figure 15 illustrates the presence of dislocation pairs throughout the microstructure. When the δ' phase is small (< 20 nm), the first dislocation passing through apparently shears the δ' phase.[59] For the peak-aged binary alloy, the δ' phase remains small enough such that the δ' phase is sheared by the dislocation (Figure 16), increasing the propensity for planar slip. As the particle coarsens and grows to sizes larger than 20 nm, as seen in the over-aged alloy, the dislocations become wavy and appear to bow around the δ' phase, eventually forming Orowan loops[60] around the δ' phase (Figure 17), resulting in softening of the alloy.[5] As expected, upon aging for 24 hrs. a δ' Al_3Li precipitate free zone develops at the grain boundaries due to the lithium depletion mechanism. This is illustrated in Figure 18.

The average grain size as a function of thermal treatment is indicated in Table III. A metallographic comparison of each microstructure is made in Figure 19. The variation of δ' diameter as a function of thermal treatment is indicated in Table IV. It can be seen that the coarsening of the spherical δ' phase follows the classical $t^{1/3}$ Ostwald ripening kinetics.

Figure 11 *Dislocations in solution treated binary alloy. Note lack of evidence of δ' precipitation.*

Figure 12 *Dislocation-δ′ interaction in under-aged binary alloy.*

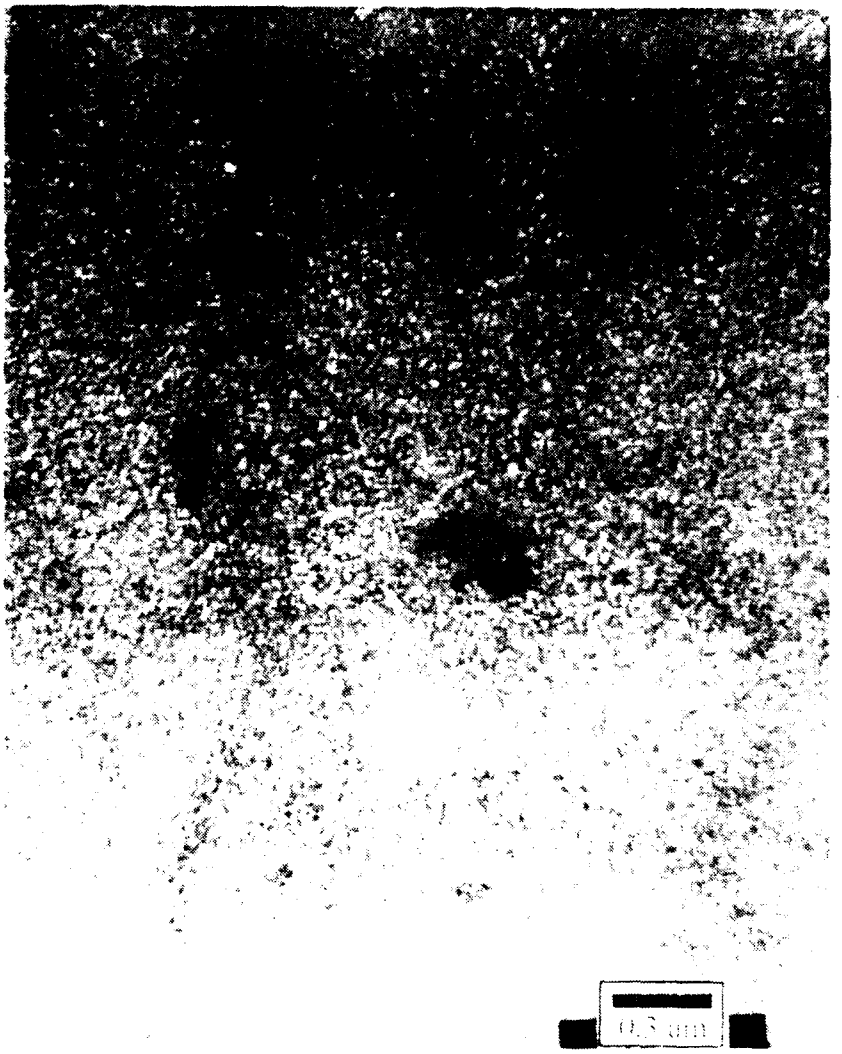

Figure 13 *Superlattice dark field image of δ' in binary Al-Li.*

Figure 14 *Coarsened δ′ precipitates in over-aged binary alloy.*

Figure 15 Superdislocation pairs in peak-aged binary alloy.

Figure 16 *Apparent dislocation-particle interaction in under-aged binary alloy. Note apparent shearing of particles.*

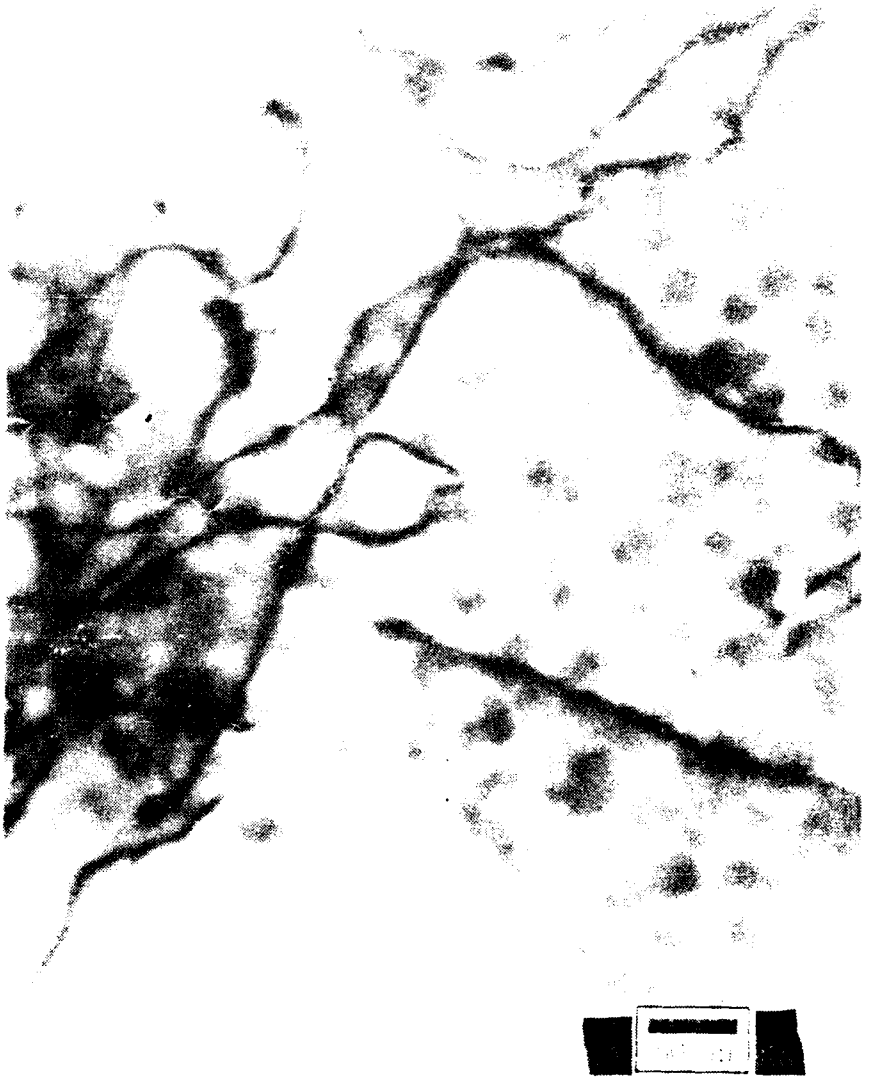

Figure 17 Over-aged binary alloy showing coarsened precipitates and possible dislocation looping.

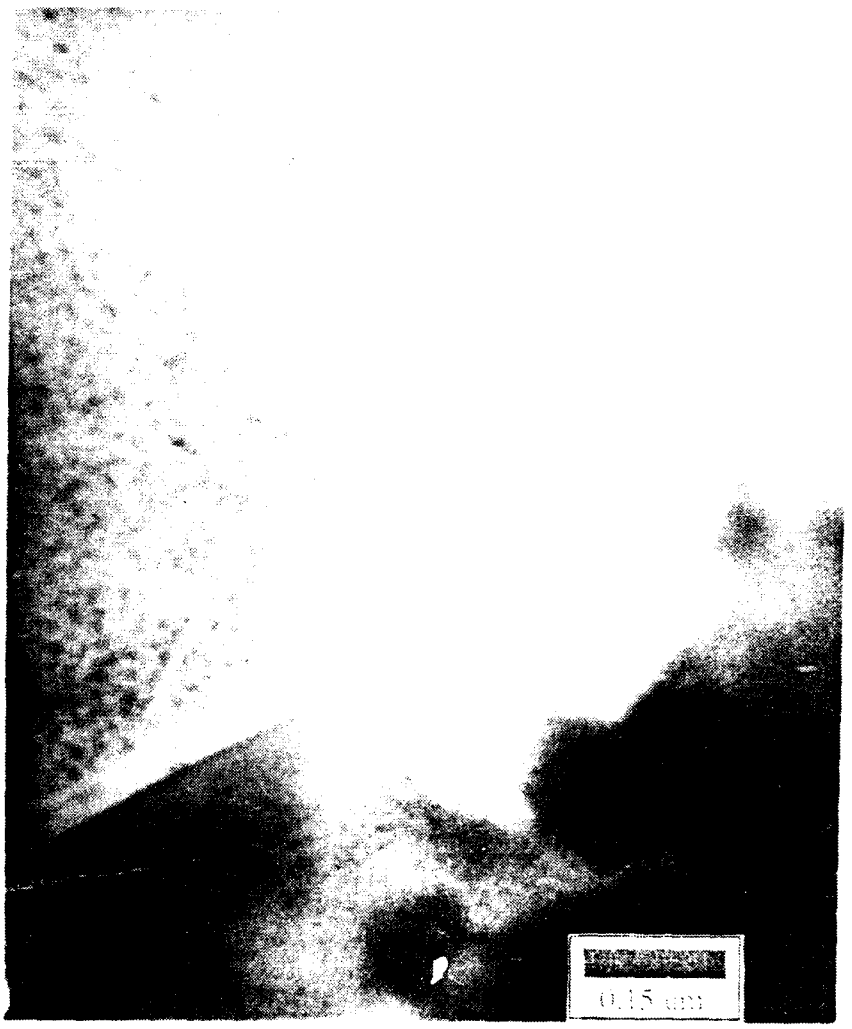

Figure 18 δ' precipitate free zone in peak-aged Al-3Li.

a

b

c

Figure 19 Optical metallography of (a) Al-3Li (b) Al-3Li-0.2Ti (c) Al-3Li-0.8Ti (200x)

TABLE III AVERAGE GRAIN SIZE VS. AGING TIME FOR BINARY Al-Li

AGING CONDITION	AVERAGE GRAIN DIAMETER (μm)
Solution-Treated	9
Under-aged	7
Peak-aged	7
Over-aged	7

TABLE IV **δ' SIZE VS. AGING CONDITION FOR BINARY Al-Li**

AGING CONDITION	δ' DIAMETER (nm)
Solution-Treated	----
Under-aged	10
Peak-aged	16.5
Over-aged	33

Al-Li-Ti Ternary Alloys

Al-3Li-0.8Ti

The Al-Li-0.8Ti alloy was solution treated at 500 C for 24 hours, followed by a water quench. In the as-quenched condition, the δ' phase precipitates as spherical coherent precipitates 8.8 nm in diameter (See Figure 20). The grains in the solution treated alloy are relatively equiaxed. After a solution treatment followed by water quench, the α' $Al_3(Li,Ti)$ phase precipitates as spherical coherent precipitates 29 nm in diameter. Selected area diffraction indicates that α' precipitates with the $L1_2$ structure.

Upon heat treating at 190 C for one hour, grains remain equiaxed with an average diameter of 5.7 μm. Precipitation of the δ' phase becomes more copious and as expected the δ' coarsens to an average size of 12 nm as shown in Figure 21.

Alloys in the peak-aged condition show an expected response to aging at 190 C for 6 hrs. The δ' coarsens to 17.4 nm. In addition to the homogeneous nucleation of the δ' in the matrix, the δ' also forms heterogeneously at the α'/matrix interface. Figure 22 shows the formation of a δ' halo around the α' $Al_3(Li,Ti)$ resulting in a composite precipitate with average diameter of 30.6 nm. In addition to the α' formation as a composite precipitate enveloped by δ', the α' also precipitates spartanly as spherical coherent precipitates. These precipitates exhibit strong matrix coherency strain contrast, which is illustrated in Figure 23.

Upon over-aging the high Ti alloy, δ' coarsens to 32 nm, while the composite precipitates achieve an average diameter of 71 nm (see Figure 24).

The dislocation behavior of the high titanium alloy is illustrated in Figure 25. The solution treated alloy exhibits a relatively high dislocation density. As aging progresses it is clear that the dislocations are again superdislocation pairs which exhibit two forms of behavior. The shearing of the δ' precipitates is observed, while dislocation bowing is also apparently observed as the coarsening reaction proceeds.

Al-3Li-0.2Ti

The addition of titanium to the Al-Li-0.2Ti alloy also alters the precipitation behavior and although α' precipitation is observed, it is not as copious as that observed in

Figure 20 *Superlattice dark field image of δ' precipitation in the as-quenched ternary alloy.*

Figure 21 δ' precipitation in under-aged ternary alloy.

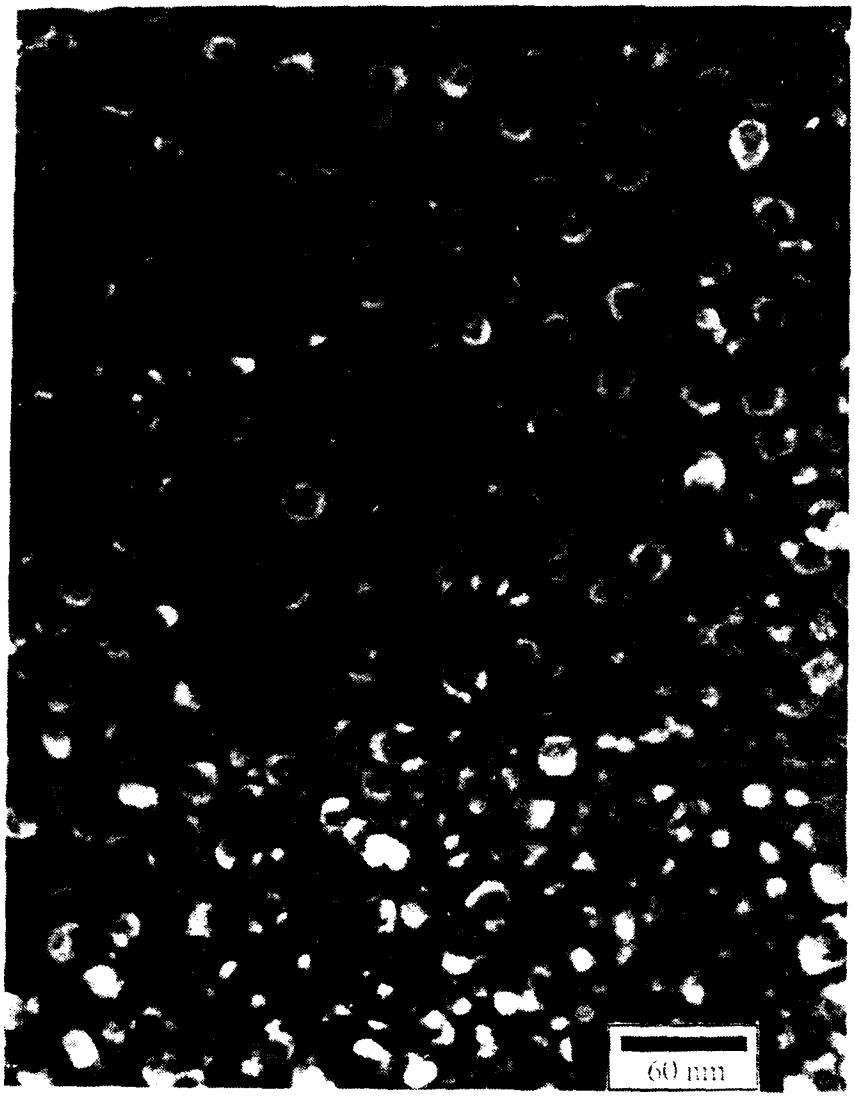

Figure 22 *Peak-aged Al-3Li-.8Ti. Note coarsening of δ' plus heterogeneous composite precipitation of δ' on α'/matrix interface.*

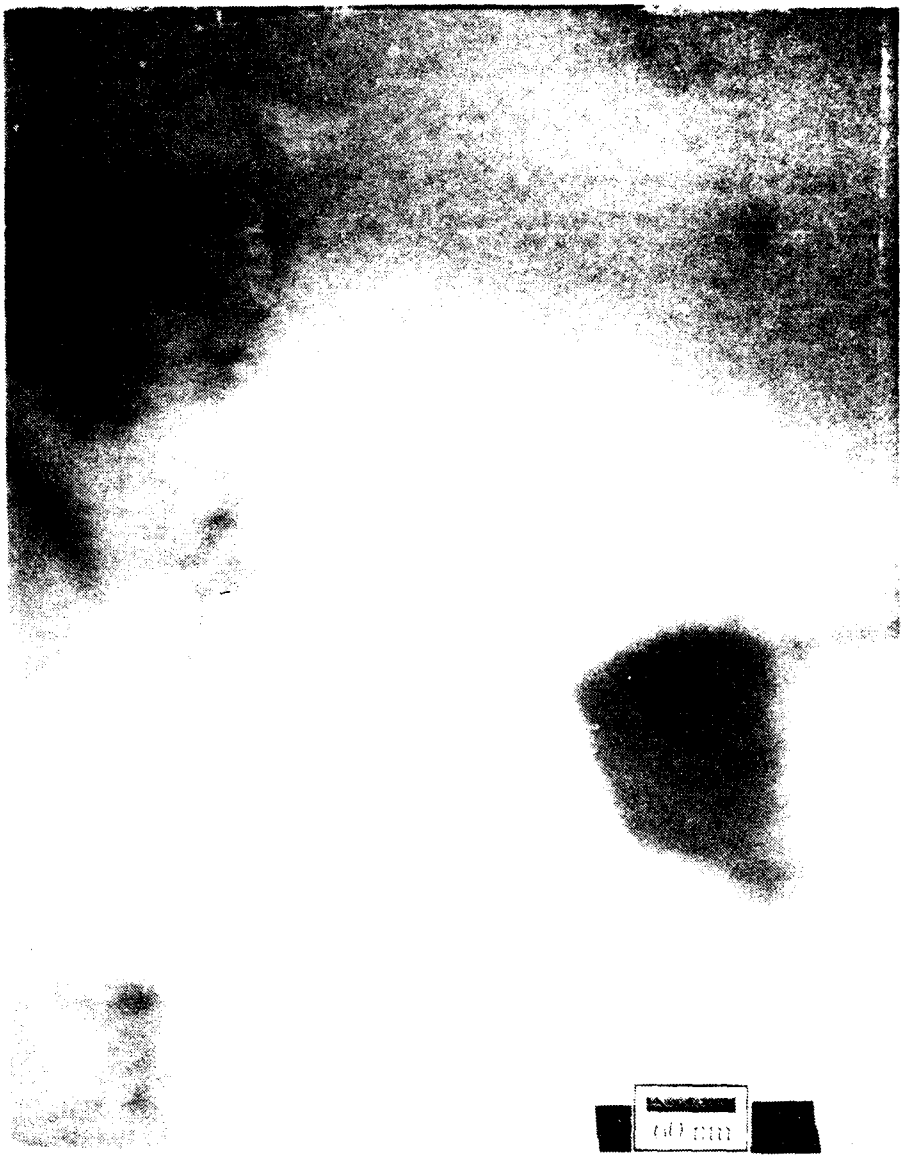

Figure 23 *α′ coherent precipitates with matrix coherency strain contrast.*

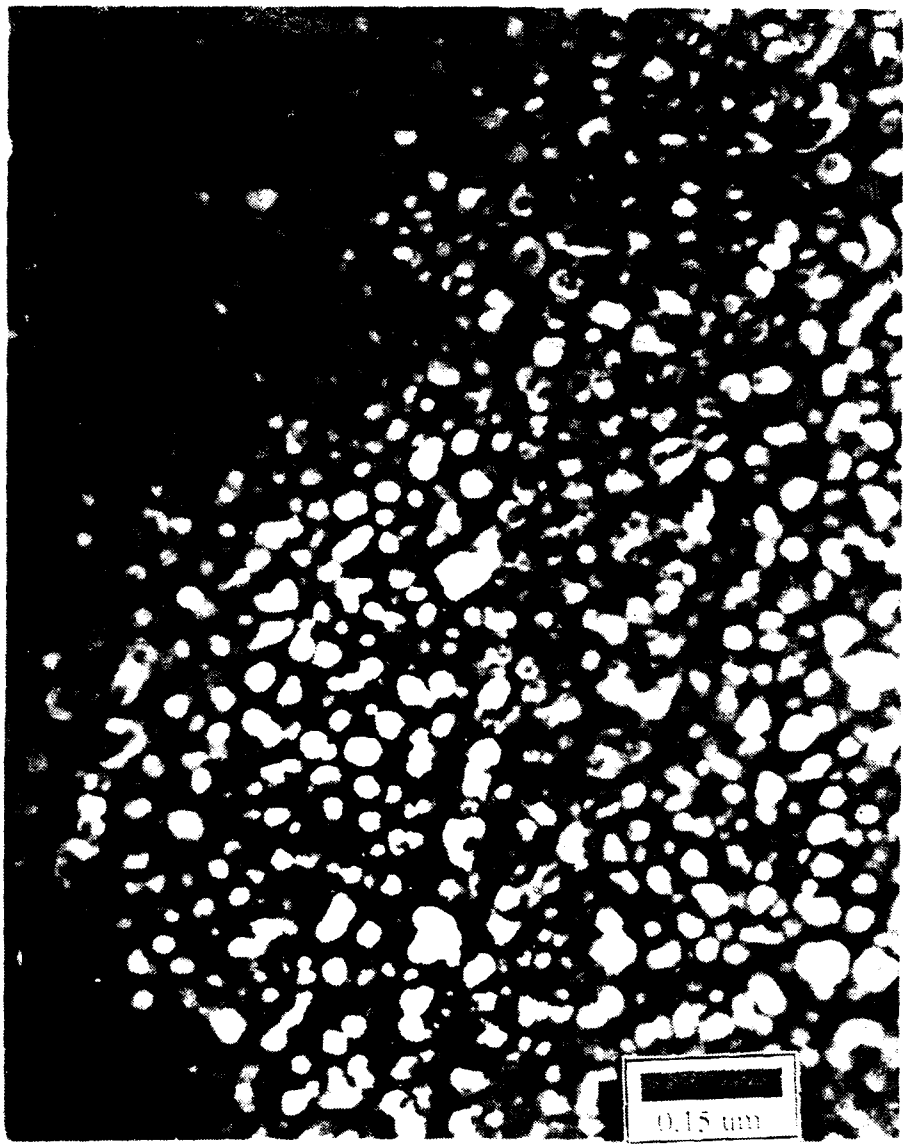

Figure 24 Coarsening of composite precipitates in over-aged alloy.

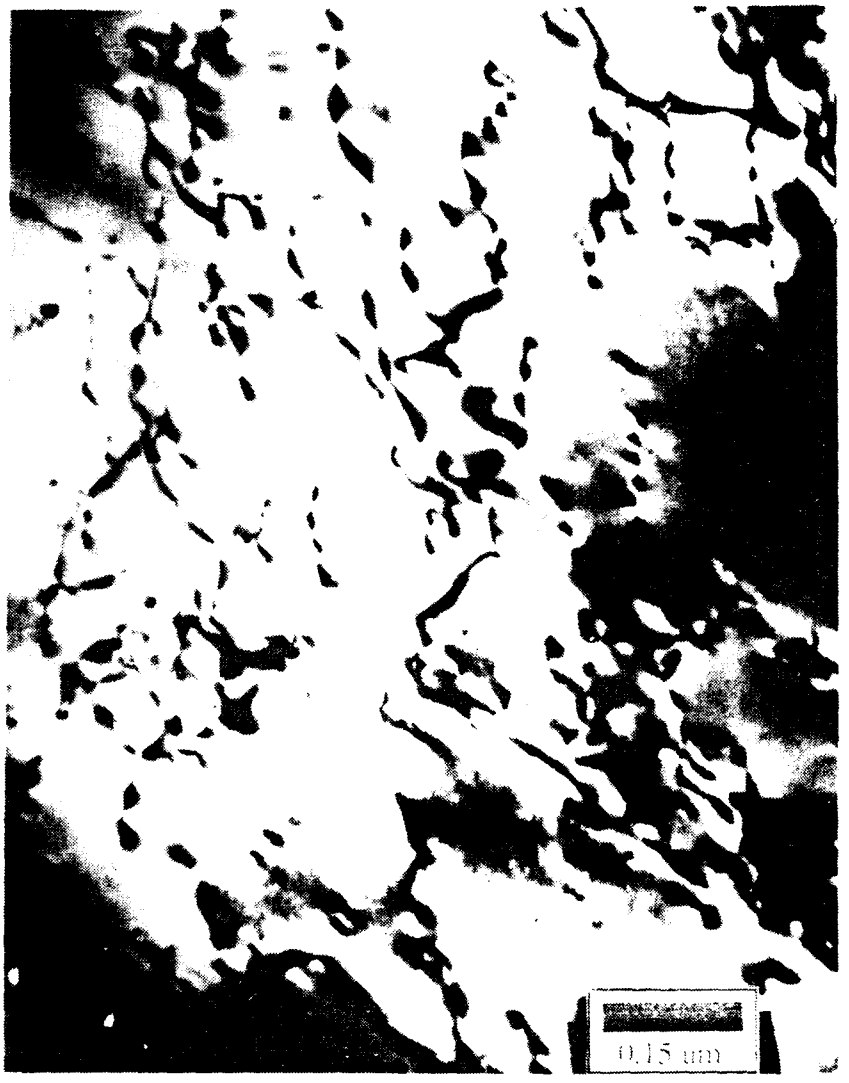

Figure 25 *Dislocation structures in ternary alloy. (a) High dislocation density in as-quenched alloy. (b) Dislocation-particle interactions - note dislocation appears to be bowing around particles.*

25b

the high titanium alloy. Upon quenching, both the α' and the δ' phases precipitate as spherical coherent precipitates (Figure 26). The average δ' size is 3.3 nm.

Upon aging, the precipitation sequence followed is much the same as that observed in the high Ti alloy, with the major difference occurring in the size and frequency of the composite precipitation. The microstructures of the low titanium containing alloys in the aged conditions can be seen in Figure 27.

In contrast to the 0.8% titanium alloy, a discontinuous coarsening reaction occurred with the homogeneously nucleated δ' precipitates. As can be seen in Figure 28 the spherical δ' phase is converted to lamellae. These lamellae, which retain coherency with the matrix, grow against the grain boundary, pushing it and causing it to bow out.

As was the case with the binary alloy, but not witnessed to such an extent in the high titanium alloy, a δ' precipitate free zone develops in the 0.2% Ti ternary alloy (Figure 29).

A relatively high dislocation density is observed in the 0.2Ti alloy in the as-quenched condition and superdislocation pairs are present in the aged specimens. Typical dislocation behavior of the Al-3Li-0.2Ti alloys is illustrated in Figure 30.

The average grain size as a function of aging treatment is listed in Table V for each of the ternary alloys. Table VI lists the δ' size and composite size as a function of aging treatment for the two ternary alloys.

Mechanical Properties

Each of the three alloys of the present study have been tested to measure tensile strength, yield strength, elongation and fracture toughness for a variety of aging conditions. It has been a goal of this research to improve the mechanical behavior and properties of aluminum-lithium alloys, particularly ductility and fracture toughness, by creating second phase particles to act as dispersoids of slip. This section reports the results of the mechanical tests performed and attempts to make a comparison of values to assess the relative properties associated with the different compositions and heat treatments.

Figure 26 *Precipitation in the as-quenched condition in Al-3Li-.2Ti.*

Figure 27 ***Precipitation response to aging in the Al-3Li-.2Ti alloy.*** *(a) Homogeneous δ' matrix precipitation as well as heterogeneous composite precipitation in the under-aged alloy. (b) Coarsening of precipitates in the peak-aged alloy. (c) Spherical coherent precipitation of α' $Al_3(Li,Ti)$.*

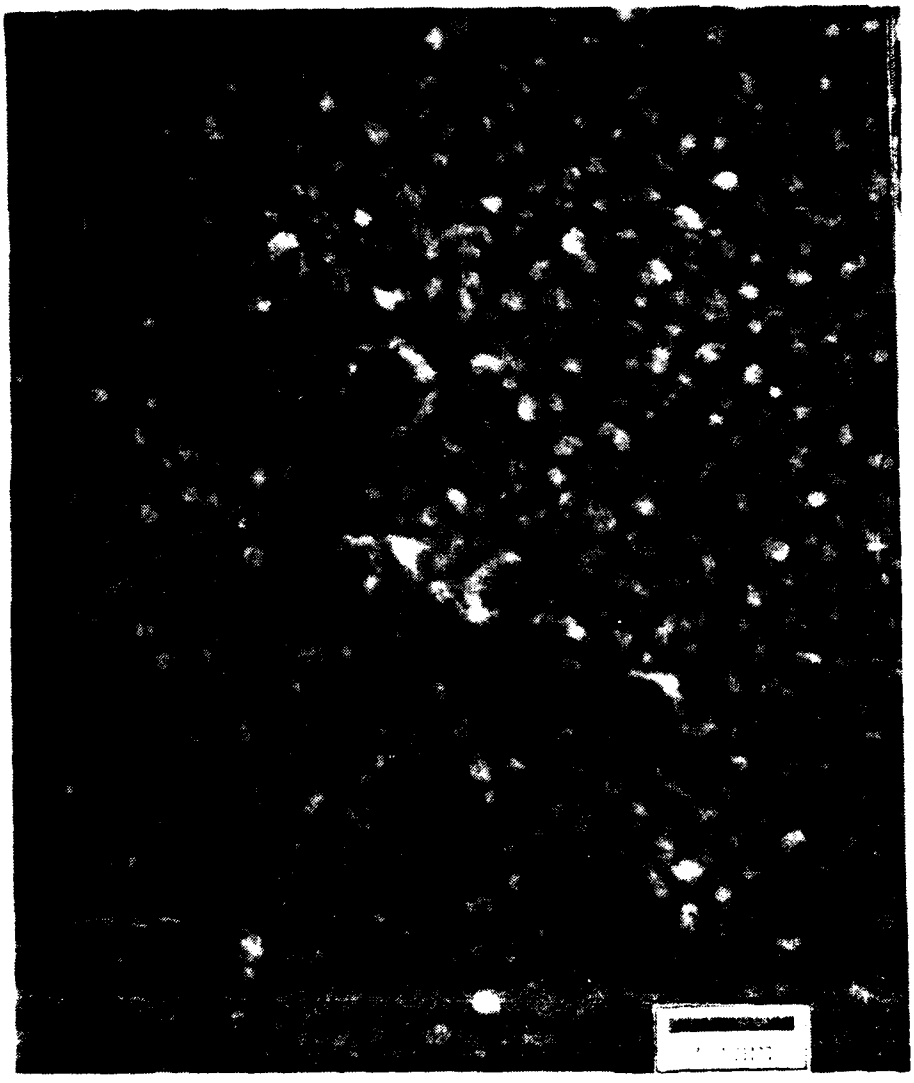

(27 b)

(27 c)

Figure 28 *Discontinuous grain boundary precipitation note conversion of δ' from sphere to lamellae and bowing of grain boundary.*

Figure 29 Development of δ' precipitate free zone.

Figure 30 Dislocation behavior in ternary alloy. Note both apparent shearing and looping of precipitates .

TABLE V AVERAGE GRAIN SIZE VS. AGING TIME FOR TERNARY Al-Li-Ti

Aging Condition	Grain Size (μm)	
	Al-Li-0.2Ti	Al-Li-0.8Ti
As - Extruded	7.2	6.2
Under-aged	5.7	5.7
Peak-aged	7.7	8.3
Over-aged	5.9	6.5

TABLE VI δ', α', AND COMPOSITE PRECIPITATE DIAMETERS VS AGING CONDITION FOR TERNARY ALLOYS

AGING CONDITION	δ' (nm) low Ti	δ' (nm) high Ti	α' (nm) low Ti	α' (nm) high Ti	COMPOSITE (nm) low Ti	COMPOSITE (nm) high Ti
Solution-Treated	3.3	8.8	—	29	—	—
Under-aged	9.5	12	30	44	—	25
Peak-aged	14	17	62	—	49	31
Over-aged	26	32	—	—	53	71

Tension Specimens

The tensile properties of the Al-3Li, Al-3Li-0.2Ti and Al-3Li-0.8Ti alloys are reported in Table VII. Properties measured include yield strength at 0.2% offset, ultimate tensile strength and elongation to failure. The results are tabulated with respect to aging treatment as well as composition. Figure 31 illustrates the response of the ultimate tensile strength to aging treatment. It is clear that tensile strength follows the trend of hardness values. Strength values in each of the three alloys reach a maximum with peak age and gradually drop in the over-aged regime. There does not appear to be any significant response of elongation to failure with aging time.

With respect to effects of composition on mechanical properties, a comparison of tensile values for each composition in the peak-aged condition is made. Figure 32 details this comparison. It is quite clear from Figure 32 that the addition of Ti to the binary P/M alloy has a significant effect on the ultimate tensile strength of each alloy. The strength increases appreciably as more Ti is added. Values obtained for elongation to failure indicate that the binary alloy exhibits better ductility than the Ti containing ternaries in the peak-aged condition (Figure 33). In the other aging conditions the ductility of the alloys is comparable. It is significant that in each case values of elongation to failure are comparable to target values established for conventional Al-Li alloys such as 2090.[23]

Fracture Toughness Bend Specimens

The values of K_Q (ksi$\sqrt{in}$) are listed in Tables VIII and IX. Tests were performed in both the L-T and the L-S directions (See Figure 34). Results are reported as the average value obtained from three specimens. Data that is not reported indicates that either the specimen broke while setting up, or cracked horizontally.

The values for K_Q are valid K_{IC} values if certain geometrical and testing parameters are met. Tables VIII and IX indicate whether these values may be reported as K_{IC}.

Fracture Surfaces

Fracture surfaces of each of the bend specimens in the solution treated and peak-aged conditions are shown in Figures 35 and 36. In the solution treated alloys, fracture is mixed. A combination of tearing and intergranular fracture is observed in the three alloys.

TABLE VII AVERAGE TENSILE PROPERTIES

SPECIMEN	.2% YIELD STRENGTH (ksi)	ULTIMATE TENSILE STRENGTH (ksi)	ELONGATION TO FAILURE %
1S	23,400	26,000	15
1U	41,380	53,605	6
1P (Al-3Li)	51,800	63,653	13
1O	50,750	62,275	5
3S	22,600	40,500	15
3U	46,705	59,285	8
3P (Al-3Li-0.2Ti)	52,004	62,152	6
3O	51.635	60,655	8
6S	30,346	43,617	14
6U	57,615	62,272	2
6P (Al-3Li-0.8Ti)	61,792	67,944	6
6O	58,660	66 338	4

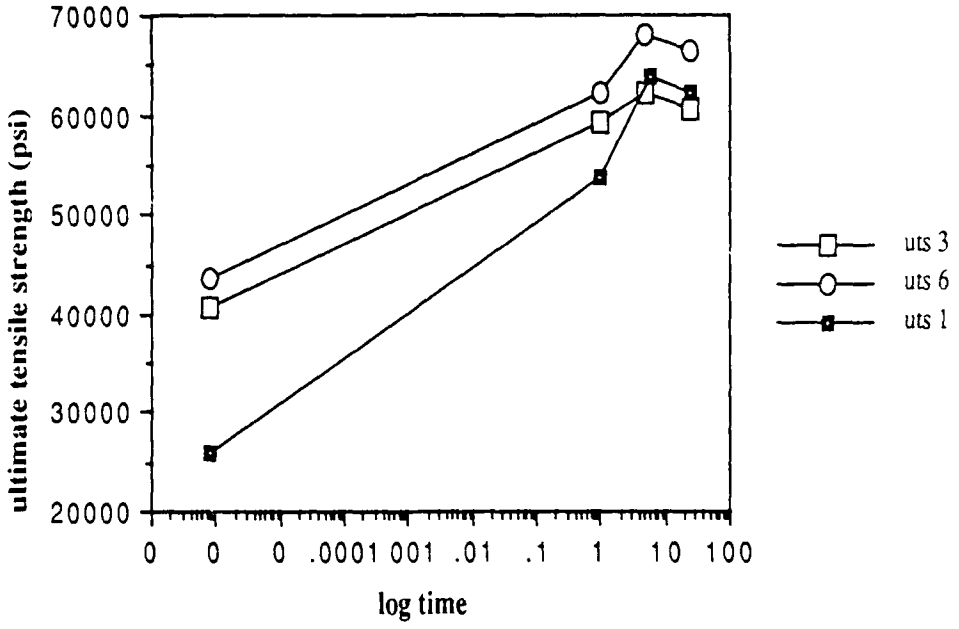

Figure 31 *Response of tensile properties of each alloy to aging treatment. (1 = Al-Li, 3 = Al-Li-.2Ti, 6 = Al-Li-.8Ti)*

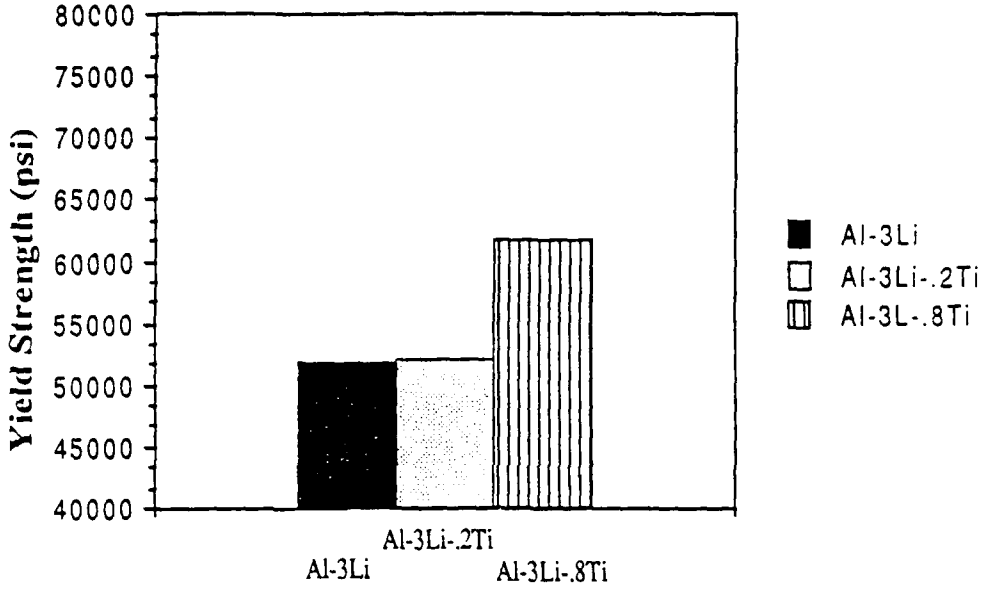

Figure 32 Yield strength of specimens in the peak aged condition.

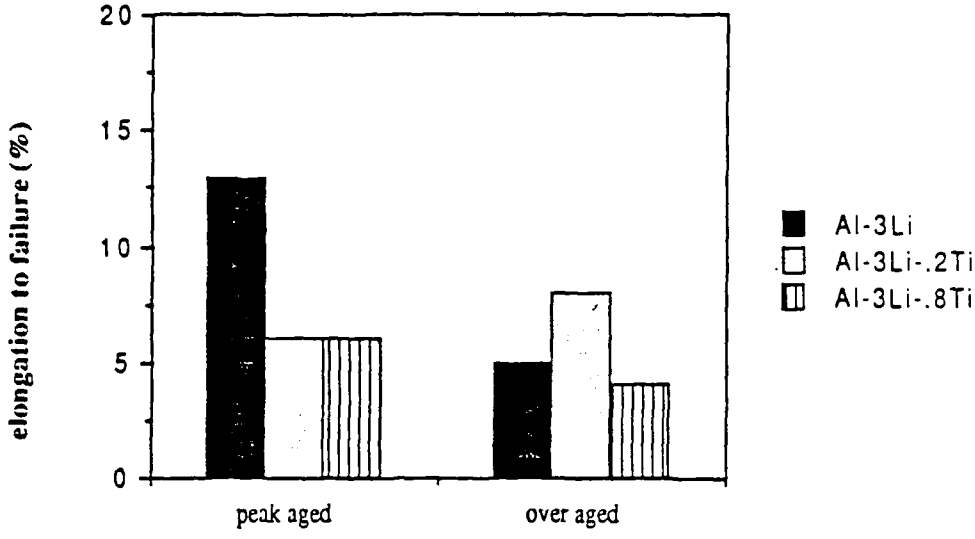

Figure 33 Elongation to failure for specimens in peak aged and over aged conditions.

TABLE VIII FRACTURE TOUGHNESS OF SPECIMENS IN THE L-T DIRECTION

SPECIMEN		K_Q	VALID K_{IC}?
1S		13.8	N
1U		19.4	Y
1P	(Al-3Li)	20.3	Y
1O		17.3	Y
3S		12.4	N
3U		15	N
3P	(Al-3Li-0.2Ti)	17.7	Y
3O		17.6	Y
6S		13.5	N
6U		14.8	Y
6P	(Al-3Li-0.8Ti)	12.5	N
6O		——	

TABLE IX FRACTURE TOUGHNESS OF SPECIMENS IN THE L-S DIRECTION

SPECIMEN		K_Q	VALID K_{IC}?
1S		15.2	N
1U		——	
1P	(Al-3Li)	19.8	N
1O		——	
3S		13.2	N
3U		20	N
3P	(Al-3Li-0.2Ti)	25	Y
3O		18.8	Y
6S		17.5	N
6U		14.1	Y
6P	(Al-3Li-0.8Ti)	15.5	N
6O		——	

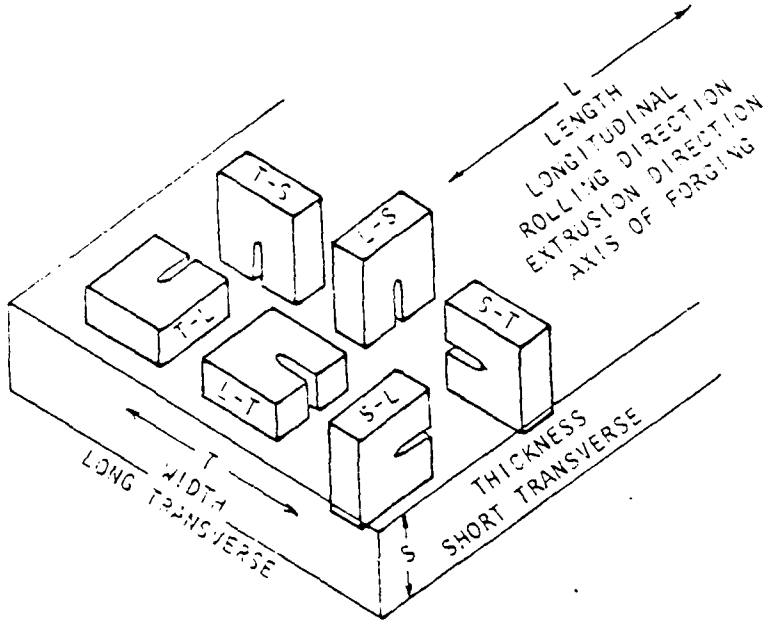

Figure 34 Crack plane orientation code for extruded bar.[78]

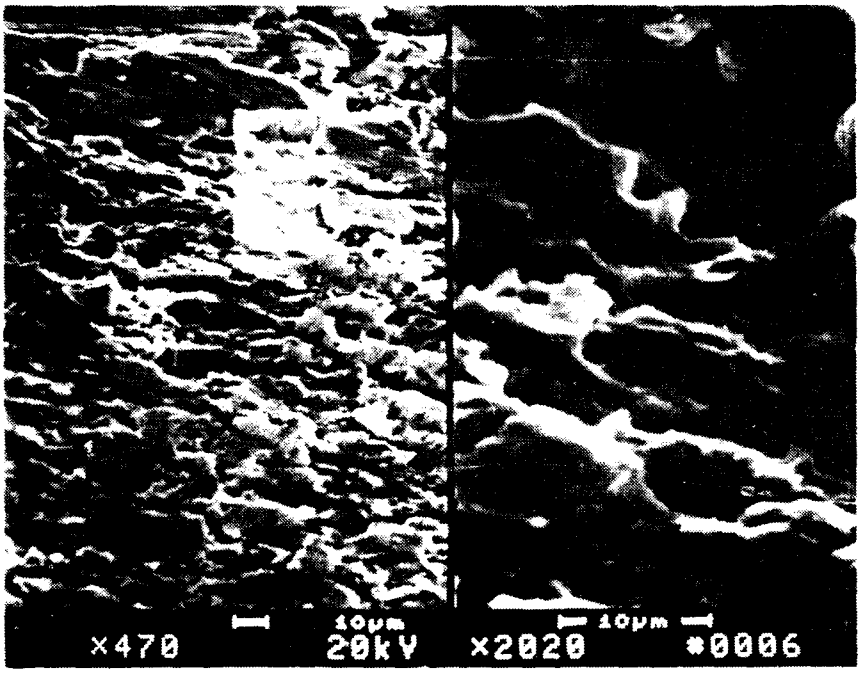

a

Figure 35 *Fracture surfaces of solution treated L-T bend specimens. (a) Al-3Li (b) Al-3Li-.2Ti (c) Al-3Li-.8Ti.*

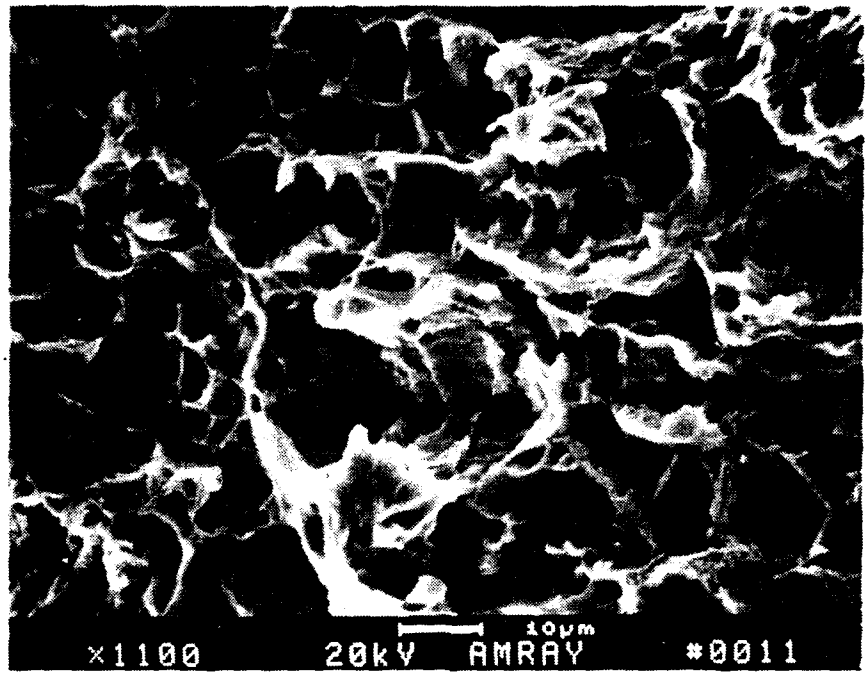

(35 b)

(35 c)

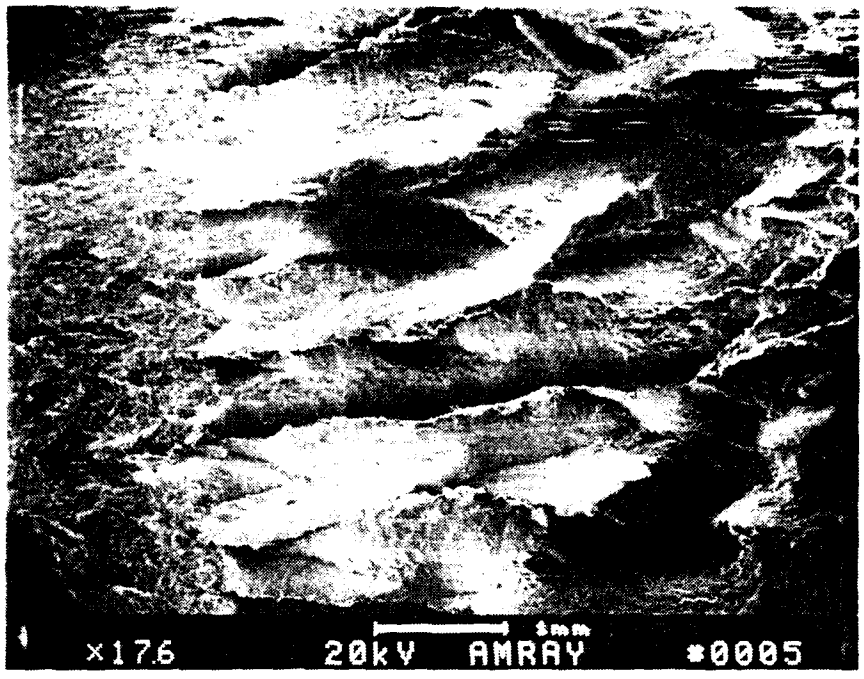

a

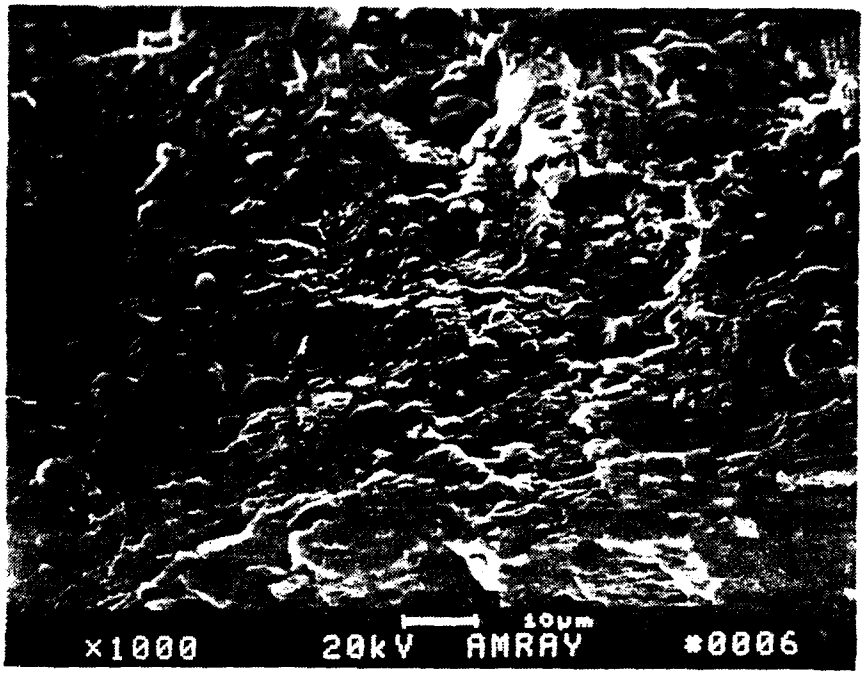

a

Figure 36 *Fracture surfaces of peak-aged L-T bend specimens. (a) Al-3Li (b) Al-3Li-.2Ti (c) Al-3Li-.8Ti*

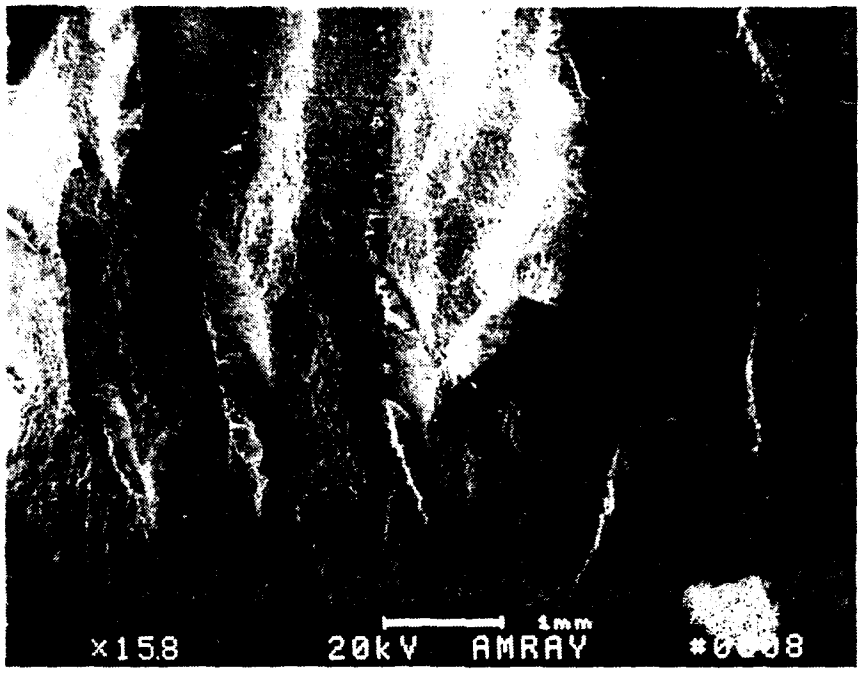

(36 b)

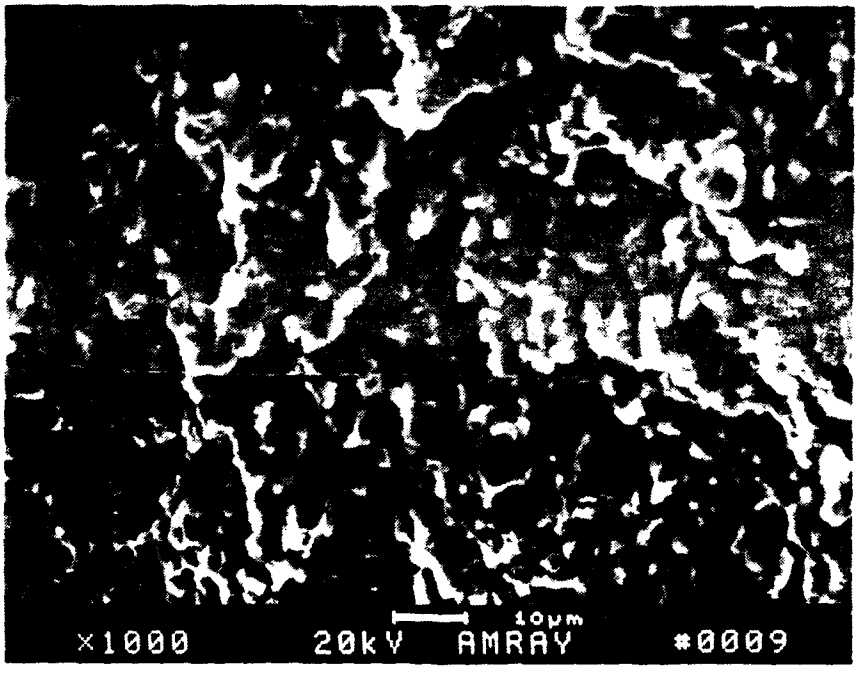

b

(36c)

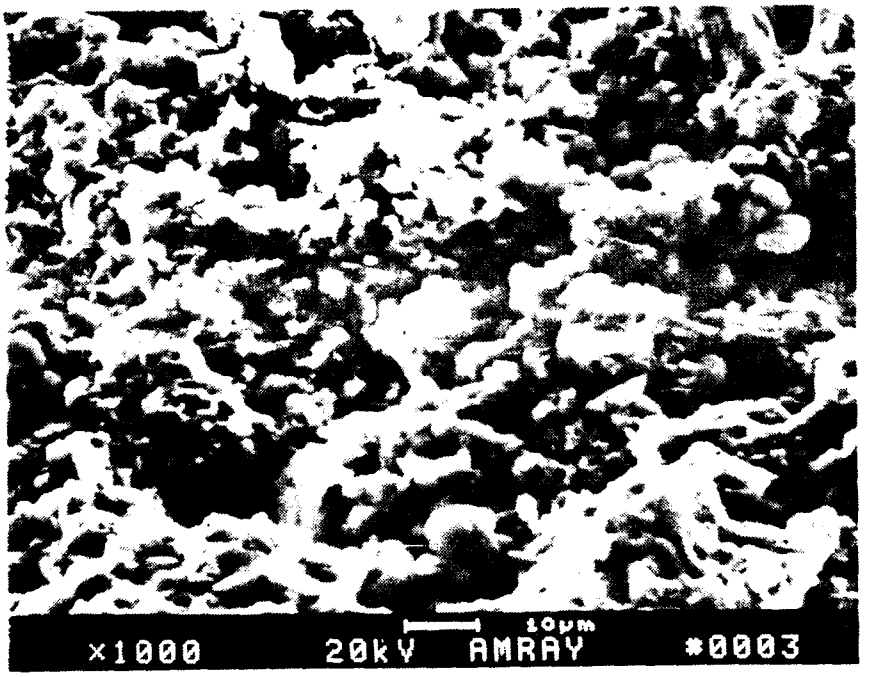

C

Fine shear lips and microdimpling are observed at grain boundaries. In the peak-aged condition, the fracture surfaces exhibit a variation for each composition. The binary alloy exhibits brittle cleavage fracture. The titanium alloys contain cleavage facets and dimples, indicating a more ductile fracture.[87]

DISCUSSION

The Binary Al-Li Alloy

The precipitation behavior in the binary Al-3Li alloy is consistent with behavior reported in studies of P/M Al-Li alloys with respect to δ' precipitation, aging behavior and coarsening.

The as-extruded binary alloy shows a homogeneous structure with no evidence of precipitation of a secondary phase. The powder metallurgical approach to the production of the binary alloy allows the incorporation of lithium contents in excess of the 2.7 wt% currently considered practical. It is therefore reasonable to assume that the Li stayed in solution throughout the vacuum-hot-compaction process and extrusion.

Precipitation During Solution Treatment

During the 500 C solution treatment the δ' remains in solid solution because the driving force for δ' to precipitate at this temperature is very low. The dislocation density in the solution treated alloys appears to be high. A probable explanation for this high dislocation density is that TEM specimen preparation processes introduce dislocations, as the foils are mechanically ground to a thickness of approximately 10 μm before they are subjected to an electropolish. It is probable that all the affected material is not removed in the final polish.

Aging And Dislocation Behavior Of Binary Alloys

Upon aging at 190 C, the driving force is sufficient to result in δ' precipitation. The δ' precipitates homogeneously in the matrix as spherical coherent precipitates with the $L1_2$ superlattice structure. Upon further aging the δ' phase coarsens according to the $r = kt^{1/3}$ Wagner-Lifshitz equation. The precipitation of the equilibrium δ (AlLi) phase at the grain boundaries results in the formation of a δ' PFZ. Because diffusion at the grain boundary is much higher than matrix diffusion, the δ phase grows at the expense of the metastable δ' phase and the PFZ develops.

It was not the intent of this thesis to fully characterize the dislocation-particle behavior of the systems, but to make observations on possible changes in behavior in response to experimental variations. Therefore the following observations made are of apparent dislocation-particle interactions. More extensive microscopy would have to be performed in order to be more quantitative. Dislocations observed to act as superdislocation pairs appear to follow classical behavior as proposed by Orowon.[60] Precipitate-dislocation interactions with and without particle shear were observed. In the initial stages of aging, small precipitates are coherent with the matrix and are therefore sheared by dislocations, with the shear stress being equivalent to:

$$\tau_{sh} = \frac{\pi \gamma r_o}{2xb}$$

where γ = Specific interface energy
r_o = Particle size
x = Particle spacing
b = Burger's vector

The stress necessary to cause dislocations to bow, and eventually form loops around particles is given as the Orowon stress:

$$\tau_{or} = \frac{Gb}{x}$$

When $\tau_{sh} > \tau_{or}$, the particles are looped, and conversely if $\tau_{sh} < \tau_{or}$, the particles are cut. As the particles increase in size, the dislocation-particle interaction apparently transforms from dislocations cutting through particles to dislocations circling around the particles.[83]

The Ternary Alloys

Al-3Li-0.2Ti / Al-3Li-0.8Ti

As-Extruded

In the microstructures observed of the as-extruded ternary alloys, there is little evidence of precipitation of a secondary phase. The process of rapid solidification is proven to be a processing technique which will increase the solid solubility of titanium in aluminum.[68,70,64,84] Equilibrium values of 0.24% Ti at 510 C have been increased to as high as 2.0% for a splat cooled alloy.[85] It is reasonable to assume, therefore, that in the presently studied Al-Li-0.2Ti and Al-Li-0.8Ti alloys produced by rapid solidification, all the titanium remained in solid solution during the extrusion process. It is observed that this was in fact the case, and little precipitation occurred throughout the vacuum-hot-compaction process.

Precipitation During Solution Treatment

As reported, it was observed that both the δ' and the α' phases precipitated following solution treatment at 500 C for 24 hours. The precipitation of the δ' phase could not be suppressed by the rapid quenching, a phenomena which in this case can be explained by the low activation energy of the δ' formation (0.7 eV).[86] The α' phase precipitated upon solution treatment in both the high and low titanium containing alloys, although more copiously in the high-Ti alloy. The twenty-four hour solution treatment parameter was previously documented as one in which sufficient precipitation of α' would occur in the form of spherical coherent precipitates.[16]

α' Phase Analysis

In order to thoroughly understand the precipitation behavior it is first necessary to determine the structure and composition of the α' precipitate. The Al-Li-Ti system can be closely compared to the Al-Ti binary system. In the binary system, the precipitating phase is Al_3Ti with the DO_{22} body-centered tetragonal structure.[67-69] The α' phase which precipitates in the ternary alloy is similar but not identical to the Al_3Ti phase.

Evidence supports the fact that the α' phase differs from the Al_3Ti phase in that it precipitates as $Al_3(Li,Ti)$. The low imaging intensity of the "core" α' phase in the superlattice dark field imaging mode indicates that lithium is mixed on the titanium sublattice, causing a decreased structure factor and therefore the lower imaging intensity. It has been observed in this study that the α' phase precipitates with a spherical shape, it is completely coherent with the aluminum matrix, a coherent strain field forms around the α', and δ' forms a continuous envelope around the α' phase. This combined evidence along with the observation that α' precipitates as the $L1_2$ structure indicate that α' is $Al_3(Li,Ti)$. If α' formed as Al_3Ti with the DO_{22} body-centered tetragonal structure it would be highly improbable that the precipitating phase, with its high lattice misfit with the aluminum matrix, would form as coherent precipitates with symmetric matrix strain fields. In addition, the assumption that α' is a lithium-modified Al_3Ti phase with a distorted lattice also is improbable because, again, distortion would prevent the formation of spherical precipitates. In all probability the α' phase with the $L1_2$ superlattice structure precipitates as $Al_3(Li,Ti)$.

It is now necessary to determine approximate values for x in the $Al_3(Li_x,Ti_{1-x})$ precipitate. Traditional methods of compositional analysis are not sufficient to provide quantitative data on the identification of the phase, essentially because the presence of lithium can not be detected by energy dispersive x-ray spectroscopy.

An excellent approximation for the composition of the α' $Al_3(Li_xTi_{1-x})$ phase can be made using a superlattice dark field imaging calculation developed by Gayle[12] and later used by Levoy[16] in her study of Al-Li-Ti and Al-Li-Hf alloys. The basic premise behind the technique is that structure factors of the superlattice reflection of the $L1_2$ ordered $Al_3(Li,Ti)$ phase are a strong function of the Li:Ti ratio. The structure factor for the superlattice reflection can be calculated and compared for various Li:Ti ratios and subsequent superlattice dark field image intensities may be obtained.

Using the fact that the δ' forms as a smooth continuous envelope on the α' core, it is possible to compose an image of a spherical composite precipitate. Levoy's[16] altered version of a computer program written by Gayle[12] makes use of inputted variables of g reflections, core composition (x in $Al_3(Li_x,Ti_{1-x})$) and the ratio R of core diameter to precipitate diameter, to produce images of composite precipitates which can then be compared to actual images with identical parameters. A value of x may then be obtained.

Using tabulated values for scattering factors and the computer program listed in Appendix A, obtained from Gayle,[12] an approximate value of 0.4-0.6 for x has been determined, indicating a range of α' composition from $Al_3(Li_{.4},Ti_{.6})$ to $Al_3(Li_{.6},Ti_{.4})$.

Aging Behavior Of Ternary Alloys

During aging at 190 C both the δ' and α' which were present in the as-quenched alloy coarsen. As was shown in Table I the diffusion of Ti in the aluminum matrix is much slower than that of Li, indicating that titanium diffusion is the rate limiting step. It is clear from the many figures that the δ' phase preferentially forms at the α'/matrix interface, resulting in a "composite" precipitate (Figure 24). At the solution treatment temperature of 500 C, there is a large driving force for titanium to precipitate, whereas the majority of lithium remains below its solubility limit. Upon aging at 190 C, both elements exceed their solubility limit and consequently precipitate. As mentioned previously, however, the diffusivity of lithium is so much higher than that of titanium that effectively, only the lithium phase precipitates and "envelopes" the titanium-rich phase which precipitated at 500 C.

The configuration of the δ' precipitates forming envelopes on α' is similar to results obtained for the Al-Li-Hf and Al-Li-Zr systems.[12,16] Both the $Al_3(Li_xTi_{1-x})$ and Al_3Li phases are of the $L1_2$ ordered structure. δ' therefore grows as a continuum of the α' phase with δ'-α' composition differences.

As was seen in Figure 29, a δ' PFZ develops along the grain boundary. The PFZ grows by a solute depletion mechanism in which solute is consumed during growth of the δ (AlLi) particle along the grain boundary.[51]

Mechanical Properties

Strengthening Behavior

It is obvious from Figure 32 that the tensile properties of the alloys studied clearly improve as titanium is added to the system. Both the ultimate tensile strength and the yield strength increase as 0.2% Ti is added and increase still further upon addition of 0.6 additional weight percent Ti.

A 7% - 68% strength increase over the binary alloys was observed in the ternary alloys. Several explanations for this behavior are possible. As titanium is added to the alloys a subsequent decrease in grain size is observed. This grain size effect, although

minimal in this case, can be directly related to increased strength through the Li equation,[83] which is an adaptation of the Hall-Petch equation[83]:

$$\delta_y = \delta_o + kd^{-1/2}$$

where σ_y = Yield stress
σ_o = Frictional stress
k = Constant
d = Grain size

which operates under the premise that grain boundaries are a source of dislocations, and the yield stress of the alloy increases with decreasing grain size.

The dominant mechanism for increasing strength with titanium addition is precipitation hardening with dislocation-particle interactions. Dislocations taking part in the deformation are confined to one set of slip planes, and these dislocations appear to expand between the particles by means of Orowon bowing. The larger and more numerous unshearable inclusions in the high-titanium alloy act as pegs that impede slip. Dislocation loops form, exert long range stresses, and increase strain hardening rates.

The α' core of the composite precipitate acts as a nondeformable particle and dislocations accumulate. The stress related to this can be approximated as

$$\tau = \tau_o + CGb\sqrt{\rho}$$

where ρ is related to the spacing between inclusions by the relation:

$$\rho = \frac{4\gamma}{Db}$$

where γ = Srain
D = Particle spacing

Therefore, as the spacing between inclusions decreases, the flow stress increases.

The strengthening afforded by the second phase precipitation is made apparent by the differences in strength among the solution treated alloys. Precipitation was observed in the two ternary solution treated alloys but not in the binary alloy. Consequently, the ternary solution treated alloys have over 60% higher tensile strength than the binary alloy with the same heat treatment.

Fracture Behavior / Scanning Electron Microscopy

Solution Treated Alloys

The fracture surfaces of the Al-3Li, Al-3Li-0.2Ti and Al-3Li-0.8Ti alloys indicate that the binary alloy undergoes a more brittle fracture than the ternaries. However the fracture toughness of the ternary alloys in certain aging conditions, as reported in Table VIII, were found to be lower than those of the binary alloy. From Figures 35 & 36 it can be seen that cleavage is the primary mode of fracture. The titanium containing alloys exhibit a combination of cleavage and tearing which indicate dimpled, ductile fracture of a softer phase in combination with a more brittle fracture of a second phase.[87] The binary alloy exhibits an intergranular fracture with shear lips and microdimpling along grain boundaries.

Peak-Aged Alloys

The fracture surfaces in each of the peak-aged alloys exhibit some degree of brittle fracture. The binary alloy fractures by cleavage. The titanium alloys have distinct fracture surfaces which exhibit combinations of cleavage and ductile fracture. The low titanium alloy appeared to have a more uniform fracture surface whereas the high titanium alloy showed definite distinct brittle and ductile regions. The high titanium alloy did not have the higher fracture toughness value that is suggested by their apparently more ductile appearance.

As is shown in Table VII, the combination of strength and elongation values of the titanium alloys are sufficiently high to indicate an expected improvement in the toughness of the ternary alloys over that of the binary alloy. There are several possible explanations as to why these improvements in fracture toughness were not realized. It has been suggested that the high titanium alloy has the fracture appearance of a composite alloy.[88] This indicates that perhaps the nondeformable second phase α' acts as a brittle composite phase. The composite precipitates occur in such a high volume fraction (Table X) in the 0.8% Ti alloy that this phase acts as a site for fracture, which would account for the lower than expected fracture toughness. In the 0.2 % titanium alloy the volume fraction of α' is

TABLE X PERCENT AREA OF SHEARABLE Li AND NON-SHEARABLE α' PHASES FOR TERNARY ALLOYS

ALLOY	% Li	$\%\alpha'$
Al-3Li-0.2Ti	55.4	36.2
Al-3Li-0.8Ti	13.5	39.3

not as high and therefore sites of fracture of the nondeformable particles are not as plentiful. The alloy subsequently exhibits a more uniform surface and a better toughness.

The ternary alloy also contained some foreign powder particles (as analyzed by EDS), of argon and boron. These were most likely introduced during processing. These impurities can act as sites for crack initiation and decrease the toughness. Oxide particles and incompletely compacted powders can also reduce the toughness. Varying processing parameters and conditions would ensure a more uniform, compacted product and give a more accurate representation of the fracture toughness of the alloy.

SUMMARY AND CONCLUSIONS

The purpose of this research was to determine how compositional variations and thermal treatments would affect microstructure and precipitation behavior of Al-Li-Ti alloys and also to determine how these variables affect the mechanical properties of the alloys. Titanium was chosen as the variable alloying element with the expectation that titanium and lithium would react to form a composite phase which would act to disperse slip and consequently increase ductility and fracture toughness of the alloys.

The precipitation behavior of the alloys is significantly altered by the addition of titanium:

1. In the binary Al-3Li alloy, δ' precipitation takes place after solution treatment and subsequent aging. δ' coarsens with $t^{1/3}$ kinetics and a δ' precipitate free zone forms after aging for five hours at 190 C.

2. Both the low and high titanium alloys exhibit similar precipitation sequences and behavior, the major difference being the volume fraction of precipitates for each alloy (Table 11).

a. δ' (Al_3Li) precipitates upon quenching in the ternary alloys.

b. α' precipitates as a coherent phase with high matrix coherency strain. The composition of this phase has been determined to be $Al_3(Li_{.6}Ti_{.4})$ by superlattice dark field image calculation.

c. Upon subsequent aging a composite phase, consisting of an α' core surrounded by δ' is formed due to the relatively rapid diffusion of lithium as compared to titanium. The composite coarsens to the size of 70 nm., which is sufficiently large to cause apparent dislocation-particle interactions to shift from dislocation shear to dislocation looping.

The mechanical properties are also dependent on the composition and thermal treatments of the alloys:

3. The strength of the alloys increases by as much as 60% from the binary to ternary alloy upon aging. It was observed, as mentioned above, that the major difference between the low and high titanium alloys was the fraction of precipitates. It is clear that this variable has a major influence on the mechanical properties of the alloys. The ternary alloys exhibit a higher strength than the binary. In addition, the high titanium alloy is stronger than the low titanium alloy due to the additional precipitation in the high titanium alloy.

4. The ductility of the alloys shows a significant response to aging. After a peak aging treatment, the binary alloy exhibits a better elongation to failure than the ternaries, although the ternary alloys still show a relatively high value. Upon further aging, the ductility of the low titanium alloy increases dramatically over the other two alloys. These results may be correlated with those obtained for fracture toughness of the alloys to conclude that the low titanium alloy has better strength/ductility combinations than the other alloys.

5. In correlating mechanical property data with fracture surfaces obtained for the bend specimens, one can conclude that the precipitation sequence of the ternary alloys does, in fact, act to impede dislocation motion, disperse slip and subsequently increase ductility. However, the non-deformable α' behave much like a brittle composite phase would and act as initiation sites for fracture. In the Al-3Li-0.8Ti alloy the volume fraction of α' is high enough to cause a dramatic decrease in the fracture toughness of the alloy.

By combining conclusions made for microstructural analysis and precipitation behavior with those made regarding mechanical properties, the following recommendations may be proposed:

1. The addition of titanium to an Al-Li alloy will result in beneficial properties only if certain parameters are met. Titanium additions of 0.8% result in much improved strength, but too large a volume fraction of non-deformable precipitates and consequently a more brittle alloy. Titanium additions of 0.2% result in improvements in fracture

toughness without significant strength improvements. It is therefore recommended that 0.4-0.5 wt% titanium be added. This amount should act to disperse slip and increase strength without precipitating to such an extent as to lower the toughness.

2. Alloys should be used in the peak-aged to slightly over-aged condition to achieve optimum combinations of results.

SUGGESTIONS FOR FUTURE RESEARCH

As has been previously established, the main driving force behind this research was to develop an Al-Li alloy which shows improvements in both fracture toughness and ductility. The approach taken in this work and those performed previously,[12,16] was to alter the precipitation behavior of the alloy in such a way as to form a slip dispersing phase which would improve mechanical properties.

Titanium has proven to show potential as the alloying element which will result in slip dispersion and subsequently increase toughness and ductility. Additional research must be performed to determine if, in fact, titanium will respond as favorably as is indicated by the present research. The major parameters which should be altered are the amounts of titanium and lithium in the alloy. Varying both the percentage lithium and that of titanium will result in drastic alterations of both the morphology and volume fraction of precipitates and should have a significant effect on toughness.

Dislocation-particle interaction plays a major role in the strengthening behavior of the alloy and should be studied much more extensively such that a more quantitative characterization of the interactions can be obtained.

Overall, an optimization study between percent lithium, percent titanium and operative aging condition should be carried out to obtain the best combination of toughness and strength and subsequently the successful integration of an Al-Li-Ti alloy into current systems.

APPENDIX A COMPUTER PROGRAM FOR COMPOSITE IMAGE CALCULATION.

```
100 REM IMAGE CALCULATIONS- COMPOSITE PPT.
1000 OPEN "O", #1, "A:COMIM8"
1100 PRINT#1, ".LH 4"
1120 PRINT#1, ".OP"
1140 PRINT#1, ".PO 0"
1210    CONTRAST = 13    'TOP (CONTRAST - 11) GRAY LEVELS ARE WHITE
1300 REM    ESTABLISH GRAY SCALE
1320     DIM GS$(15)
1340     FOR GN = 0 TO 15
1350     READ GS$(GN)
1360     NEXT GN
1370     DATA A, B, C, D, E, F, G, H, I, J, K, L, M, N, O, P
1500 REM  ** FIGURE STRUCTURE FACTORS FOR DELTA PRIME AND AL3TI **
1520     DIM F(1,20)
1540     FOR N=0 TO 1
1560        FOR I = 1 TO 20
1570        READ F(N,I)
1580     NEXT I:NEXT N
1590 REM  STRUCTURE FACTOORS FOR THE BINARY PHASES - FIRST AL3TI, THEN AL3LI
1592 REM       FOR REFLECTIONS N=2 = 1,2,3,4,..... FOR SUPERLATTICE
1594 REM       REFLECTIONS. (INDICATED AS 0 IF FUNDAMENTAL)
1595 DATA 1.76,0,0,0,0,0,0,0,0,0
1596 DATA 0,0,0,0,0,0,0,0,0,0
1597 DATA -2.72,0,0,0,0,0,0,0,0,0
1598 DATA 0,0,0,0,0,0,0,0,0,0
2000 REM ** ASCERTAIN NO. OF IMAGES AND CALCULATE **
2020 READ  NUMIM       'NUMBER OF IMAGES
2100 REM  ** CALCULATE IMAGE **
2120     DIM LS(40)
2200     FOR ITER = 1 TO NUMIM
2220     READ RATIO        'FRACTION OF TOTAL RADIUS DOUBLE PRIME
2240     RE=1000:  RC = 1000*RATIO 'RADIUS TOTAL, RADIUS CORE FOR IM CALC
2260     READ COMP         'X IN AL3(LIx,Til-x) core
2280     READ REFL         'IMAGING REFLECTION
2300     READ R        'TRUE TOTAL PPT RADIUS FOR TOTAL IM INTENSITY
2500 PRINT#1, "COMPOSITE PRECIPITATE"
2510 PRINT #1,
2520 PRINT#1, "  CORE IS DELTA' ', Al3(Lix,Til-x), WHERE xIS ";COMP
2525 PRINT#1,
2540 PRINT#1,"     CORE RADIUS = ",R*RATIO; "NM"
2545 PRINT#1,
2546 PRINT#1,"      TOTAL PARTICLE RADIUS = ";R;"NM"
2547 PRINT#1,
2550 PRINT#1, "IMAGING SUPERLATTICE REFLECTION IS";REFL
2555 PRINT#1,
2560 PRINT#1, "(CONTRAST LEVEL IS";CONTRAST;", 12 IS ONE LEVEL OF WHITE)"
2565 PRINT#1,
2570 PRINT#1, "@"
2575 REM   IN ABOVE THE "@" WILL BE CHANGED TO A "CONTROL Y", WHICH
2576 REM   IS USED TO GO INTO GRAYSCALE MODE.
```

```
2600     A=REFL        'HKL
2610     B = INT(REFL/10)          'HK
2620     C = INT(REFL/100)         'H
2630     N = ((A/10-B)*10)^2+((B/10-C)*10)^2+C^2      'H^2+K^2+L^2="N"
2640     FP= F(1,N)          'STRUCTURE FACTOR DELTA PRIME
2650     FDP = F(0,N)*(1-COMP) + F(1,N)*COMP      'F ALPHA PRIME
2800 REM  FIGURE SCALING INTENSITTY IMAX
2820     IMAX = 0 :Y = 0
2840     FOR X=0 TO 1070 STEP 5
2860     IF X^2 =RC^2 THEN ZCT = 0 ELSE ZCT = (RC^2-X^2)^(.5)
2870     IF X^2 =RE^2 THEN ZET = 0 ELSE ZET = (RE^2-X^2)^(.5)
2880              TDP = 2*ZCT: TP = 2*(ZET-ZCT)
2890              I = (TP*FP+TDP*FDP)^2
2900     IF ABS(I) > ABS (IMAX) THEN IMAX = I
2920     NEXT X
3000 REM    CALCULATE IMAGE
3010     FOR Y = 0 TO 1060 STEP 27
3015         L = Y/27
3020             LS(L) = ""
3040     FOR X = -1080 TO 1070 STEP 27
3050        XYS = X^2 + Y^2
3060     IF XYS  =RE^2 THEN I=0:GOTO 5000
3080     ZET = (RE^2-XYS)^(.5)
3100     IF XYS  =RC^2 THEN I = (2*ZET*FP)^2: GOTO 5000
3120     ZCT = (RC^2-XYS)^(.5)
3140     TDP = 2*ZCT       'THICKNESS ALPHA PRIME
3160     TP = 2*(ZET-ZCT)      'THICKNESS DELTA PRIME
3180     I = (TP*FP+TDP*FDP)^2    'INTENSITY FOR S=0
5000     GS = CINT(ABS((I/IMAX)*CONTRAST))
5020     LS(L)=LS(L) + GS$(GS)
5030 NEXT X
5060     NEXT Y
5500 FOR L = -40 TO 40
5520     PRINT#1, LS(ABS(L))
5540 NEXT L
6000 PRINT#1,
6004 PRINT#1,"@"          'REPLACE @ WITH ^Y B4 WS PRINTING
6005 PRINT#1, "IMAX = ";IMAX
6050 PRINT#1,
6110 PRINT#1, "IMAX * R^2 =";IMAX*R^2
6120 PRINT#1, ".PA"
6140 PRINT ITER;"IMAGES DONE AND SENT HOME-ONLY";NUMIM-ITER "LEFT"
6200 NEXT ITER
7000 END
7900 REM
7950 REM THE FOLLOOWING ARE INPUT DATA
7960 REM R-VALUE, "X" (COMPOSITION OF CORE), REFLECTION
7970 REM  RADIUS OF TOTAL COMPOSITE PPT IN NM
8000 DATA 1
8040 DATA .440, .8,100, 71
9000 DATA 0,0,0,0,0,0,0,0,0,0,0,0
```

APPENDIX A COMPOSITE IMAGE CALCULATION

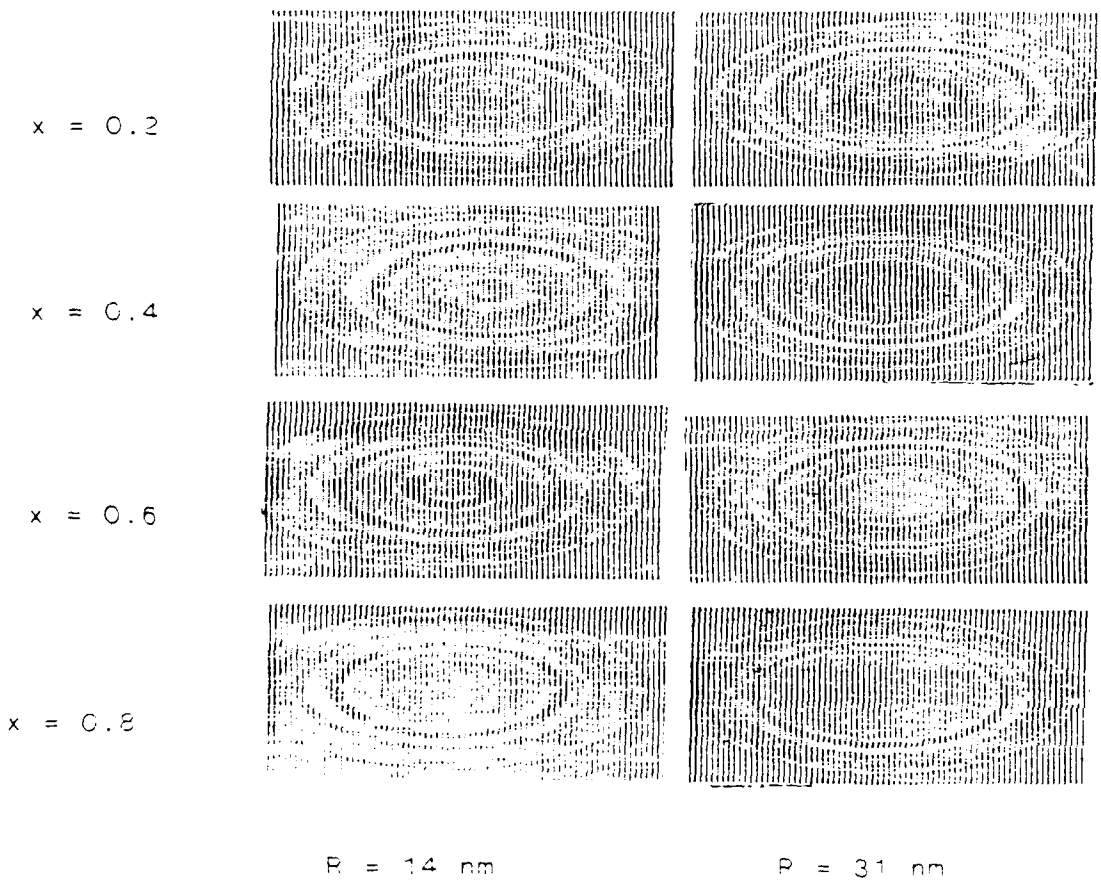

g = 100

BIBLIOGRAPHY

1. **Aluminum-Lithium Alloys**, (eds. T.H. Sanders. Jr. and E.A. Starke Jr.), TMS-AIME, New York, (1981).

2. **Aluminum-Lithium Alloys II**, (eds. T.H. Sanders. Jr. and E.A. Starke Jr.), TMS-AIME, New York, (1984).

3. K. Dinsdale, S.J. Harris and B. Noble: **Aluminum-Lithium Alloys**, (eds. T.H. Sanders. Jr. and E.A. Starke Jr.), TMS-AIME, New York, (1981), 101.

4. B. Noble, S.J. Harris and K. Dinsdale: J. Mat. Sci., 17, (1982), 461.

5. T.H. Sanders Jr. and E.A. Starke Jr.: Acta Metall., 31, (1982), 927.

6. F.W. Gayle: **Aluminum-Lithium Alloys**, (eds. T.H. Sanders. Jr. and E.A. Starke Jr.), TMS-AIME, New York, (1981), 119.

7. T.H. Sanders Jr.: "Factors Influencing Fracture Toughness and Other Properties of Al-Li Alloys," Naval Air Development Center, Contract No. N62269-76-C-0271, Final report, June 14, 1979.

8. T.H. Sanders Jr.: Materials Science and Engineering, 43, (1980), 247.

9. M. Tamura, T. Mori and T. Nakamura: Trans. JIM, 14, (1973), 335.

10. B. Noble, S.J. Harris and K. Dinsdale: Metal Science, 16, (1982), 425.

11. M. Tamura, T. Mori and T. Nakamura: J. JIM, 34, (1970), 919.

12. F.W. Gayle: Sc.D. thesis, Massachusetts Institute of Technology, 1985.

13. I.G. Palmer, R.E. Lewis and D.D. Crooks: **Aluminum-Lithium Alloys**, (eds. T.H. Sanders. Jr. and E.A. Starke Jr.), TMS-AIME, New York, (1981), 241.

14. C.J. Peel, B. Evans, C. Baker, D.A. Bennett, P.J. Gregson and H.M. Flower: **Aluminum-Lithium Alloys II**, (eds. T.H. Sanders Jr. and E.A. Starke Jr.) TMS-AIME,New York, (1984), 363.

15. J.W. Bohlen and G.R. Chanani: **Aluminum-Lithium Alloys II**, (eds. T.H. Sanders Jr. and E.A. Starke Jr.) TMS-AIME,New York, (1984), 407.

16. N.F. Levoy: Sc.D. thesis, Massachusetts Institute of Technology, 1986.

17. H.K. Hardy and J. M. Silcock: J. Inst. Met., 84, (1955-56), 423-428.

18. H.K. Hardy: J. Inst. Met., 84, (1955-56), 429-439.

19. P. Vachet: French Patent No. 1,161,306, Application date 1956, Granted 1958.

20. E.S. Balmuth and R. Schmidt: **Aluminum-Lithium Alloys**, (eds. T.H. Sanders Jr. and E.A. Starke Jr.) , (1981), 69-87.

21. I.N. Fridlyander, N.V. Shiryaeva, S.M. Ambartsumyan, T.A. Gorokhova, R.M. Gabidullin, N.G. Sidorov, N.A. Sorokin and A.N. Kuznetsov: U.K. Patent No. 1,172,736, Application date 1967, granted 1969, and French Patent No. 1,519,021, Application date 1967, granted 1968.

22. T. Yoshi-Yama and K. Hasebe: J. Phys. Soc. Japan, 25, (1968), 908.

23. J.R. Pickens, K. Kumar and T.J.Langan: Technical Report under Army Materials Technology Laboratory contract number DAAG46-85-C-0034., 1987.

24. P.E. Bretz and R.R. Sawtell: **Aluminum-Lithium Alloys III,** (eds. C. Baker, P.J. Gregson, S.J. Harris and C.J. Peel) The Institute of Metals, London, (1986), 47-56.

25. C.J. Peel, B. Evans and D. McDarmaid: ibid., 26-36.

26. P. Meyer and B. Dubost: ibid, 37-46.

27. E.A. Starke Jr., T.H. Sanders Jr. and I.G. Palmer: Journal of Metals, (1981), 24-32.

28. A. Collier: Metal Weekly News, Sept. 19, (1988), 56.

29. B. Noble and G.E. Thompson: Met.Sci. J., 5, (1971), 114.

30. A.J. McAlister: Bulletin of Alloy Phase Diagrams, 3, (1982), 177-183.

31. G. Cocco, G. Fagherazzi, and L. Schiffini: J. Appl. Cryst., 10, (1977), 325-327.

32. F.W. Gayle and J.B. VanderSande: Bulletin of Alloy Phase Diagrams, 5, (1984), 19-20.

33. J. Buth and G. Inden: Acta Metall., 30, (1982), 213-224.

34. J.M. Silcock: J. Inst. Metals, 88, (1959), 359.

35. D.B. Williams and J.W. Edington: Met. Sci. J., 9, (1975), 529.

36. S.F. Baumann and D. B.Williams: Scripta Met., 18, (1984), 611-616.

37. F. Livet and D. Bloch: Scripta Met., 10, (1985), 1147-1151.

38. I.N. Fridlyander, V.S. Sandler and T.I. Nikol'skaya: Fiz. Met. Metall., 32, (1971), 767-774.

39. L.N. Trofimova and K.V. Chuistov: Phys. Met. Metall., 44, (1978), 99-103.

40. S. Ceresara, A. Giarda and A. Sanchez: Phil. Mag., 35, (1977), 97-110.

41. M.A. Vasil'yev, A.A. Kosyachkov, L.N. Trofimova, V.T. Cherepin and K.V. Chuistov: Phys. Met. Metall., 45, (1979), 197-199.

42. F.S. Lin, S.B. Chakrabortty and E.A. Starke Jr.: Met. Trans. A., 13A, (1982), 401-410.

43. D.B. Williams: **Aluminum-Lithium Alloys**, (eds. T.H. Sanders Jr. and E.A. Starke Jr.), (1981), 89-99.

44. D. Venables, L. Christodoulou and J.R. Pickens: Scripta Met., 17, (1983), 1263-1268.

45. K. Mahalingam, B.P. Gu, G.L. Liedl and T.H. Sanders Jr.: Acta Metall., 35, (1987), 483-498.

46. P.J. Gregson and H.M. Flower: J. Mat. Sci. Letters, 3, (1984), 829-834.

47. B. Gu: Dissertation Abstracts International, 46, (1986), 3973-B.

48. D.B. Williams and J.W.Edington: Acta Metall., 24, (1976), 323-332.

49. J.M. Silcock: J. Inst. Met., 88, (1960), 357.

50. P. Niskanen, T.H. Sanders Jr., M. Marek and J.G. Rinker: **Aluminum-Lithium Alloys**, (eds. T.H. Sanders. Jr. and E.A. Starke Jr.), TMS-AIME, New York, (1981), 347.

51. S.C. Jha, T.H. Sanders Jr. and M.A. Dayananda: Acta Metall., 35, (1987), 473-482.

52. N.J. Grant, S. Kang and W. Wang: **Aluminum-Lithium Alloys**, (eds. T.H. Sanders Jr. and E.A. Starke Jr.) , (1981), 171-187.

53. W.R.D. Jones and P.P Das: J. Inst. Metals, 88, (1959), 435-443.

54. D. Webster: **Aluminum-Lithium Alloys**, (eds. T.H. Sanders Jr. and E.A. Starke Jr.) , (1981), 228-239.

55. M. Peters, J. Eschweiler and K. Welpmann: Scripta Met., 20, (1986), 259-264.

56. D. Webster, G. Wald and W.S. Cremens: Met. Trans. A., 12A, (1981), 1495-1502.

57. J. De Hosson and A.Veld: Acta Metall., 32, (1984), 1205-1215.

58. T.H. Sanders Jr., E.A. Ludwiczak and R.R. Sawtell: Mat. Sci. and Eng., 43 (1980), 247-260.

59. M. Furukawa,Y. Miura and M. Nemoto: Trans. JIM, 26, (1985), 225-229.

60. E. Orowon: **Dislocations in Metals**, AIME Publication, (1954).

61. J. Tarnacki and Y. Kim: Scripta Met., 22, (1988), 329-334.

62. M.D. Eborall: J. Inst. Metals, 76, (1949-50), 295.

63. T. Sato, S. Den and G. Ohira: Trans. JIM, 20, (1979), 687-696.

64. T. Ohasi and R. Ichikawa: Z. Metallkde, 64, (1973), 517-521.

65. L. Arnberg, L. Backerud and H. Klang: Metals Technology, (1982), 14-17.

66. L. Arnberg, L. Backerud and H. Klang: Metals Technology, (1982), 7-13.

67. L. Arnberg, L. Backerud and H. Klang: Metals Technology, (1982), 1-6.

68. K. Asboll and N. Ryum: J. Inst. Metals, 101, (1973), 212.

69. H.A.F. El Halfawy: **Titanium '80--Science and Technology** (Proceedings of the Fourth International Conference on Titanium), Kyoto, Japan, May 19-22, (1980), 1379.

70. V.I. Dobatkin, et. al.,: Russian Metallurgy (Metally), 2, (1970), 122.

71. H.A. Lipsitt, D. Shechtman and R.E. Schafrik: Met. Trans. A., 11A, (1980), 1369.

72. J.C. Williams and M.J. Blackburn: **Ordered Alloys**, (ed. H. Kear, T. Sims, S. Stoloff and J.H. Westbrook), Claitor's Publishing Division, Baton Rouge, LA, (1970), 425.

73. S.M.L. Sastry and H.A. Lipsitt: Acta Met., 25, (1977), 1279.

74. W.E. Frazier and M.J. Kaczak: Scripta Met, 21, (1987), 129-134.

75. S.A. Court, M.H. Loretto and H.L. Fraser: Scripta Met., 21, (1987), 997-1002.

76. K.K. Sankaran, S.M.L. Sastry and J.E. O'Neal: **Aluminum-Lithium Alloys**, (eds. T.H. Sanders Jr. and E.A. Starke Jr.) , (1981), 189-203.

77. C. Baker, P.J. Gregson, S.J. Harris and C.J. Peel, (eds.): **Aluminum-Lithium Alloys III**, The Institute of Metals, London, (1986)

78. R.E. Pasternak, M.S. Pepi, G.P. Pelletier, C.W. Amos and M.D. Valvanis: Army Materials Technology Laboratory Technical Report, MTL SP 87-5, (1987), 9.

79. R.E. Pasternak, M.S. Pepi, G.P. Pelletier, C.W. Amos and M.D. Valvanis: Army Materials Technology Laboratory Technical Report, MTL SP 87-5, (1987), 11.

80. H. Vosskuhler: Metallwirtscharft, 16, (1937), 907.

81. C.L. Angerman : J. Nuc. Mat., 11, (1964), 41.

82. T. Yoshi-Yama, K. Hasebe and M. Mannami: J. Phys. Soc. Japan, 25, (1968), 908.

83. M.A. Meyers and K.K. Chawla: **Mechanical Metallurgy Principles and Applications.**, Prentice-Hall, Inc., Englewood Cliffs, N.J., (1984).

84. V.I. Dobatkin, V.I. Elagin and V.M. Fedorov: Russian Metallurgy, 5, (1969), 107.

85. J. Bletry: J. Phys. Chem. Solids, 31, (1970), 1263.

86. M.A. Vasil'yev, A.A. Kosyachkov, L.N. Trofimova, V.T. Cherepin and K.V.Chuistov: Phys. Met. Metall., 45, (1979), 197-199.

87. J.A. Fellows, Chairman: **Metals Handbook: Fractography and Atlas of Fractographs**, 9, 8th edition, (1974).

88. Private Conversation with Ernest S.C. Chin.

89. W.G. Moffatt: **The Handbook of Binary Phase Diagrams**, Genium Publishing Corp., N.Y., (1976) .

No. of Copies	To
	Commander, U.S. Army Aeromedical Research Unit, P.O. Box 577, Fort Rucker, AL 36360
1	ATTN: Technical Library
	Commander, U.S. Army Aviation Systems Command, Aviation Research and Technology Activity, Aviation Applied Technology Directorate, Fort Eustis, VA 23604-5577
1	ATTN: SAVDL-E-MOS
	U.S. Army Aviation Training Library, Fort Rucker, AL 36360
1	ATTN: Building 5906-5907
	Commander, U.S. Army Agency for Aviation Safety, Fort Rucker, AL 36362
1	ATTN: Technical Library
	Commander, USACDC Air Defense Agency, Fort Bliss, TX 79916
1	ATTN: Technical Library
	Commander, U.S. Army Engineer School, Fort Belvoir, VA 22060
1	ATTN: Library
	Commander, U.S. Army Engineer Waterways Experiment Station, P. O. Box 631, Vicksburg, MS 39180
1	ATTN: Research Center Library
	Commandant, U.S. Army Quartermaster School, Fort Lee, VA 23801
1	ATTN: Quartermaster School Library
	Naval Research Laboratory, Washington, DC 20375
1	ATTN: Code 5830
2	Dr. G. R. Yoder - Code 6384
	Chief of Naval Research, Arlington, VA 22217
1	ATTN: Code 471
1	Edward J. Morrissey, AFWAL/MLTE, Wright-Patterson Air Force, Base, OH 45433
	Commander, U.S. Air Force Wright Aeronautical Laboratories, Wright-Patterson Air Force Base, OH 45433
1	ATTN: AFWAL/MLC
1	AFWAL/MLLP, M. Forney, Jr.
1	AFWAL/MLBC, Mr. Stanley Schulman
	National Aeronautics and Space Administration, Marshall Space Flight Center, Huntsville, AL 35812
1	ATTN: R. J. Schwinghammer, EH01, Dir, M&P Lab
1	Mr. W. A. Wilson, EH41, Bldg. 4612
	U.S. Department of Commerce, National Institute of Standards and Technology, Gaithersburg, MD 20899
1	ATTN: Stephen M. Hsu, Chief, Ceramics Division, Institute for Materials Science and Engineering
1	Committee on Marine Structures, Marine Board, National Research Council, 2101 Constitution Ave., N.W., Washington, DC 20418
1	Librarian, Materials Sciences Corporation, Guynedd Plaza II, Bethlehem Pike, Spring House, PA 19477
1	The Charles Stark Draper Laboratory, 68 Albany Street, Cambridge, MA 02139
	Wyman-Gordon Company, Worcester, MA 01601
1	ATTN: Technical Library
	Lockheed-Georgia Company, 86 South Cobb Drive, Marietta, GA 30063
1	ATTN: Materials and Processes Engineering Dept. 71-11, Zone 54
	General Dynamics, Convair Aerospace Division, P.O. Box 748, Fort Worth, TX 76101
1	ATTN: Mfg. Engineering Technical Library
1	Mechanical Properties Data Center, Belfour Stulen Inc., 13917 W. Bay Shore Drive, Traverse City, MI 49684
1	Mr. R. J. Zentner, EAI Corporation, 626 Towne Center Drive, Suite 205, Joppatowne, MD 21085-4440
	Director, U.S. Army Materials Technology Laboratory, Watertown, MA 02172-0001
1	ATTN: SLCMT-TML
1	Author

DISTRIBUTION LIST

No. of Copies	To
1	Office of the Under Secretary of Defense for Research and Engineering, The Pentagon, Washington, DC 20301
	Commander, U.S. Army Laboratory Command, 2800 Powder Mill Road, Adelphi, MD 20783-1145
1	ATTN: AMSLC-IM-TL
1	AMSLC-CT
	Commander, Defense Technical Information Center, Cameron Station, Building 5, 5010 Duke Street, Alexandria, VA 22304-6145
2	ATTN: DTIC-FDAC
1	Metals and Ceramics Information Center, Battelle Columbus Laboratories, 505 King Avenue, Columbus, OH 43201
	Commander, Army Research Office, P.O. Box 12211, Research Triangle Park, NC 27709-2211
1	ATTN: Information Processing Office
	Commander, U.S. Army Materiel Command, 5001 Eisenhower Avenue, Alexandria, VA 22333
1	ATTN: AMCLD
	Commander, U.S. Army Materiel Systems Analysis Activity, Aberdeen Proving Ground, MD 21005
1	ATTN: AMXSY-MP, H. Cohen
	Commander, U.S. Army Missile Command, Redstone Scientific Information Center, Redstone Arsenal, AL 35898-5241
1	ATTN: AMSMI-RD-CS-R/Doc
1	AMSMI-RLM
	Commander, U.S. Army Armament, Munitions and Chemical Command, Dover, NJ 07801
2	ATTN: Technical Library
1	AMDAR-LCA, Mr. Harry E. Pebly, Jr., PLASTEC, Director
	Commander, U.S. Army Natick Research, Development and Engineering Center, Natick, MA 01760
1	ATTN: Technical Library
	Commander, U.S. Army Satellite Communications Agency, Fort Monmouth, NJ 07703
1	ATTN: Technical Document Center
	Commander, U.S. Army Tank-Automotive Command, Warren, MI 48397-5000
1	ATTN: AMSTA-ZSK
2	AMSTA-TSL, Technical Library
	Commander, White Sands Missile Range, NM 88002
1	ATTN: STEWS-WS-VT
	President, Airborne, Electronics and Special Warfare Board, Fort Bragg, NC 28307
1	ATTN: Library
	Director, U.S. Army Ballistic Research Laboratory, Aberdeen Proving Ground, MD 21005
1	ATTN: SLCBR-TSB-S (STINFO)
	Commander, Dugway Proving Ground, Dugway, UT 84022
1	ATTN: Technical Library, Technical Information Division
	Commander, Harry Diamond Laboratories, 2800 Powder Mill Road, Adelphi, MD 20783
1	ATTN: Technical Information Office
	Director, Benet Weapons Laboratory, LCWSL, USA AMCCOM, Watervliet, NY 12189
1	ATTN: AMSMC-LCB-TL
1	AMSMC-LCB-R
1	AMSMC-LCB-RM
1	AMSMC-LCB-RP
	Commander, U.S. Army Foreign Science and Technology Center, 220 7th Street, N.E., Charlottesville, VA 22901
1	ATTN: Military Tech

U.S. Army Materials Technology Laboratory,
Watertown, Massachusetts 02172-0001
THE EFFECT OF COMPOSITION AND AGING TREATMENT ON THE MICROSTRUCTURE AND MECHANICAL PROPERTIES OF ALUMINUM-LITHIUM-TITANIUM ALLOYS -
Marietta R. Cappucci

Technical Report MTL TR 89-78, August 1989, 99 pp - illus-tables, D/A Project 1L162105.AH84

AD_____

UNCLASSIFIED
UNLIMITED DISTRIBUTION

Key Words

Aluminum-lithium-titanium alloys
Lightweight alloys
Microstructure

Aluminum-lithium alloys have recently been recognized for their potential as aerospace alloys. Al-Li alloys offer the combination of high strength and elastic modulus with low density, thereby resulting in substantial weight and cost savings. The precipitation of the metastable δ'(Al_3Li) phase upon aging provides considerable increases in strength. The major problem encountered thus far is that the δ' phase, due to its shearable nature, causes slip localization, reducing ductility and fracture toughness. The present study is based on the theory that by altering the precipitation behavior and characteristics by additions of titanium it will be possible to disperse slip and consequently increase fracture toughness. Titanium has been selected as the alloying element because in the Al-Ti binary system Al_3Ti forms with lattice parameter and crystal structure similar to those of Al_3Li. Al-3Li, Al-3Li-0.2Ti and Al-3Li-0.8Ti (wt%) alloys were processed using powder metallurgy and were extruded. Microstructural characterization at various age hardening conditions has been carried out. A ternary $Al_3(Li,Ti)$ phase, designated α', precipitates upon solution heat treatment at 500 C for 24 hours. α' precipitates as a coherent ordered precipitate with high matrix coherency strain. Upon aging, δ' precipitates both homogeneously in the matrix and heterogeneously at the α'/matrix interface, forming a "composite" precipitate consisting of an α' core surrounded by δ'. The technique of superlattice dark field image calculation has been used to determine the composition of the $Al_3(Li_x,Ti_{1-x})$ phase. The value for x has been determined to be ~ 0.4 - 0.6. The mechanical properties of the alloys have been determined at several aging conditions. The strength of the alloy increases significantly at each aging condition as titanium is added to the system. Elongation to failure remains fairly constant with titanium additions, but fracture toughness drops as higher amounts of titanium are added. The Al-3Li-0.2Ti alloy shows the best combination of strength and toughness.

U.S. Army Materials Technology Laboratory,
Watertown, Massachusetts 02172-0001
THE EFFECT OF COMPOSITION AND AGING TREATMENT ON THE MICROSTRUCTURE AND MECHANICAL PROPERTIES OF ALUMINUM-LITHIUM-TITANIUM ALLOYS -
Marietta R. Cappucci

Technical Report MTL TR 89-78, August 1989, 99 pp - illus-tables, D/A Project 1L162105.AH84

AD_____

UNCLASSIFIED
UNLIMITED DISTRIBUTION

Key Words

Aluminum-lithium-titanium alloys
Lightweight alloys
Microstructure

Aluminum-lithium alloys have recently been recognized for their potential as aerospace alloys. Al-Li alloys offer the combination of high strength and elastic modulus with low density, thereby resulting in substantial weight and cost savings. The precipitation of the metastable δ'(Al_3Li) phase upon aging provides considerable increases in strength. The major problem encountered thus far is that the δ' phase, due to its shearable nature, causes slip localization, reducing ductility and fracture toughness. The present study is based on the theory that by altering the precipitation behavior and characteristics by additions of titanium it will be possible to disperse slip and consequently increase fracture toughness. Titanium has been selected as the alloying element because in the Al-Ti binary system Al_3Ti forms with lattice parameter and crystal structure similar to those of Al_3Li. Al-3Li, Al-3Li-0.2Ti and Al-3Li-0.8Ti (wt%) alloys were processed using powder metallurgy and were extruded. Microstructural characterization at various age hardening conditions has been carried out. A ternary $Al_3(Li,Ti)$ phase, designated α', precipitates upon solution heat treatment at 500 C for 24 hours. α' precipitates as a coherent ordered precipitate with high matrix coherency strain. Upon aging, δ' precipitates both homogeneously in the matrix and heterogeneously at the α'/matrix interface, forming a "composite" precipitate consisting of an α' core surrounded by δ'. The technique of superlattice dark field image calculation has been used to determine the composition of the $Al_3(Li_x,Ti_{1-x})$ phase. The value for x has been determined to be ~ 0.4 - 0.6. The mechanical properties of the alloys have been determined at several aging conditions. The strength of the alloy increases significantly at each aging condition as titanium is added to the system. Elongation to failure remains fairly constant with titanium additions, but fracture toughness drops as higher amounts of titanium are added. The Al-3Li-0.2Ti alloy shows the best combination of strength and toughness.

U.S. Army Materials Technology Laboratory,
Watertown, Massachusetts 02172-0001
THE EFFECT OF COMPOSITION AND AGING TREATMENT ON THE MICROSTRUCTURE AND MECHANICAL PROPERTIES OF ALUMINUM-LITHIUM-TITANIUM ALLOYS -
Marietta R. Cappucci

Technical Report MTL TR 89-78, August 1989, 99 pp - illus-tables, D/A Project 1L162105.AH84

AD_____

UNCLASSIFIED
UNLIMITED DISTRIBUTION

Key Words

Aluminum-lithium-titanium alloys
Lightweight alloys
Microstructure

Aluminum-lithium alloys have recently been recognized for their potential as aerospace alloys. Al-Li alloys offer the combination of high strength and elastic modulus with low density, thereby resulting in substantial weight and cost savings. The precipitation of the metastable δ'(Al_3Li) phase upon aging provides considerable increases in strength. The major problem encountered thus far is that the δ' phase, due to its shearable nature, causes slip localization, reducing ductility and fracture toughness. The present study is based on the theory that by altering the precipitation behavior and characteristics by additions of titanium it will be possible to disperse slip and consequently increase fracture toughness. Titanium has been selected as the alloying element because in the Al-Ti binary system Al_3Ti forms with lattice parameter and crystal structure similar to those of Al_3Li. Al-3Li, Al-3Li-0.2Ti and Al-3Li-0.8Ti (wt%) alloys were processed using powder metallurgy and were extruded. Microstructural characterization at various age hardening conditions has been carried out. A ternary $Al_3(Li,Ti)$ phase, designated α', precipitates upon solution heat treatment at 500 C for 24 hours. α' precipitates as a coherent ordered precipitate with high matrix coherency strain. Upon aging, δ' precipitates both homogeneously in the matrix and heterogeneously at the α'/matrix interface, forming a "composite" precipitate consisting of an α' core surrounded by δ'. The technique of superlattice dark field image calculation has been used to determine the composition of the $Al_3(Li_x,Ti_{1-x})$ phase. The value for x has been determined to be ~ 0.4 - 0.6. The mechanical properties of the alloys have been determined at several aging conditions. The strength of the alloy increases significantly at each aging condition as titanium is added to the system. Elongation to failure remains fairly constant with titanium additions, but fracture toughness drops as higher amounts of titanium are added. The Al-3Li-0.2Ti alloy shows the best combination of strength and toughness.